KERNFORSCHUNGSZENTRUM

KARLSRUHE

November 1968

KFK 878
EUR 4158 e

Institut für Angewandte Reaktorphysik

Theoretical and Computer Analysis on the Behaviour of Fast Reactor Fuel Pins and Related Parts of the Core under Operational Conditions

G. Karsten, H. Kämpf, A. Gerken
with Contribution of
M. Guyette

GESELLSCHAFT FUR KERNFORSCHUNG M. B. H.

KARLSRUHE

KERNFORSCHUNGSZENTRUM KARLSRUHE

November 1968

KFK-878
EUR 4158 e

Institut für Angewandte Reaktorphysik

Theoretical and Computer Analysis on the Behaviour of Fast Reactor Fuel Pins and Related Parts of the Core under Operational Conditions *

G. Karsten, H. Kämpf, A. Gerken
with Contribution of
M. Guyette **

Gesellschaft für Kernforschung mbH, Karlsruhe

* Work performed within the association in the field of fast reactors between the European Atomic Energy Community and Gesellschaft für Kernforschung mbH, Karlsruhe

** Belgonucléaire-Delegate

Contents

1. Introduction

The maximum operation times of the fuel pins of a power reactor are of especially great importance for the economy of the reactor core. Therefore a great number of burnup irradiation experiments are performed. Theoretical efforts have been done to optimize the design of irradiation experiments. This was supported by an evaluation of numerous reports on irradiation and basic experiments. Thus a development of a theoretical basis of fuel pin operation behaviour and correspondingly a theoretically founded, generally valid, fuel pin design was started.

In this work a study of the maximum operation times of the fuel pins was made by following the reference design study on the Sodium Cooled Fast Breeder Reactor Na-2. As the basis of this examination there was taken a defined three zone volume balance relating to the swelling of fuel volume and the consumption of void volume, given by the hot gap volume, the axial expansion and ratios of the pore volume. To calculate the maximum burnup with this model the radial temperature distribution had to be treated quantitatively. For doing this a new porosity relationship of the thermal conductivity was used, which was developed recently. Furthermore a two zone porosity model was applied for the characterization of the porosity migration in the plastic region connected with the central channel formation and a densification in the plastic region. The used zone swelling rates and applied availability factors were argued. The still unsolved fuel clad interaction problem was characterized and discussed. To initiate the quantitative treatment of the interaction problem a multiaxial stress and strain evaluation of the creeping sheath was carried out by an iterative method.

2. Theoretical assumptions

2.1. Formulation of the burnup model

The basis of this study is the "burnup formula" <1,2> in the following modified form

$$A_{max} = \frac{P_o(G_{pl}\cdot V_{pl} + G_{cr}\cdot V_{cr} + G_{lt}\cdot V_{lt}) + V_{hg} + V_{ax}}{(1 - P_o)(S_{pl}\cdot V_{pl} + S_{cr}\cdot V_{cr} + S_{lt}\cdot V_{lt})} \qquad (1)$$

This formula is basing on the following model: The space within the clad of a fuel pin is divided into three annular temperature zones, the "plastic zone" for temperatures above $T_{pl} = 1700^{o}C$, the "creep zone" for temperatures between $T_{pl} = 1700^{o}C$ and $T_{cr} = 1300^{o}C$ and the "low temperature zone" for temperatures below $T_{cr} = 1300^{o}C$. The maximum burnup A_{max} is reached, if in an axial volume element of the space within the clad the fuel volume produced in the three zones according to specific constant swelling rates S_{pl}, S_{cr} and S_{lt} has filled the given void volume without interaction with the cladding. This is valid under provision of a free displaceability of the fuel. It is assumed furthermore, that the void volume is realized on the one hand by the original porous volume, which is given by the porosity P_o and which is available in the three fuel zones according to specific constant availability factors G_{pl}, G_{cr} and G_{lt}. On the other hand the swelling fuel can fill the hot gap volume V_{hg} and can partially expand in axial direction with the volume V_{ax}.

A = burnup $\quad \frac{MWd}{t(\text{heavy elements})}$

$S = \frac{1}{A}\frac{\Delta V}{V_{th}}$ = swelling rate $\quad \frac{v/o\ (\text{theoretical dense})}{10^4\ \frac{MWd}{t(\text{heavy elements})}} = 10^{-6}\ \frac{t}{MWd}$

V_{th} = volume of the theoretical dense fuel

V_i = volumes
G_i = availability factors
} i = pl, cr, lt

P_o = initial, (as-fabricated) porosity

The maximum operation time t_{max} is combined with the maximum burnup A_{max} in the following way

$$t_{max} = \frac{\pi \rho_h r_f^2 (1 - P_o)}{\chi} \cdot A_{max} \qquad (2)$$

t_{max} = maximum operation time
ρ_h = density of the heavy elements of the theoretical dense fuel
r_f = fuel radius
χ = linear rod power

Considering (1) and (2) we can see that the maximum operation time varies within the core with respect to the linear rod power χ, the temperature volumes V_{pl}, V_{cr}, V_{lt} and V_{hg} which are given by the temperature distribution. This is calculated in chapter 2.2. Furthermore the maximum operation time is given by the swelling rates, the availability factors and the axial volume expansion. These values are discussed in chapter 2.3. and 2.4.

2.2. Calculation of the temperature volumes and of the hot gap volume

2.2.1. Porosity dependence of the thermal conductivity

The following relation for isotropic porosity distribution was developed on the base of a mixing model <3>

$$k(T,P) = k_{th}(T)\left[1 - P^{\frac{2}{3}}\left(1 - \frac{1}{1 + P^{\frac{1}{3}}\left(\frac{k_{th}}{k_p} - 1\right)}\right)\right] \qquad (3)$$

k = thermal conductivity of the porous ceramic fuel
k_{th} = thermal conductivity of the theoretical dense fuel
k_p = thermal conductivity of the pores
T = temperature
P = porosity

The heat transfer in the pore is caused by heat conductivity and temperature radiation. In <3> the following formula was derived:

$$k_p = C_{cond}\sqrt{T_p} + C_r T_p^3 d\,ß \qquad (4)$$

C_{cond} = material property for thermal conduction
C_r = material property for temperature radiation
d = largest length of the pore in direction of the heat flow
ß = shape factor
T_P = temperature of the pore

From (3) and (4) results the following approximation

$$k(T,P) = k_{th}(T)\left[1 - P^{\frac{2}{3}}\right] \qquad (5)$$

which is valid for all practically interesting temperatures and gas contents of the pores and for sufficient small pore sizes, e.g. for Xenon (5) is valid for pore sizes smaller than 40 µ.

(5) is represented graphically in fig. 1. If the curve (5) is replaced by Loebs' straight lines varying rises in succeeding porosity sections are obtained.

$$k(T,P) = k_{th}(T)\left[1 - \eta P\right] \qquad (6)$$

η = constant relating to linear porosity relation

For $0 < P < 0,1$ $\eta = 2,5$
$0,1 < P < 0,15$ $\eta = 2$
$0,15 < P < 0,25$ $\eta = 1,7$

We realize that the thermal conductivity rises more than proportionally with decreasing porosity. These results theoretically obtained are in a very good agreement with experimentally found results ⟨4 to 10⟩, especially the big value of the constant η at small porosities. Contrary to these results Biancheria ⟨11, 12⟩ theoretically obtained an opposite direction of the factors i.e. a small value η for small porosities. Biancheria's results based on a publication ⟨13⟩ about the "Mathematical treatment of the electric conductivity and capacity of disperse systems". There is either an error in this work or the translation of this electric case into the thermal case is impossible.

2.2.2. Thermal dependence of the thermal conductivity

To get the temperature dependence of the thermal conductivity of the theoretical dense fuel $k_{th}(T)$ the results of the following authors ⟨14 to 20⟩ are averaged. These results are relating to stoichiometric UO_2 respectively $(U_{0,8}Pu_{0,2})O_2$ with 95 % of theoretical density. The corresponding values of the theoretical dense fuel follow from the porosity relation (5). These were adjusted according to the method of least squares with the equation

$$k_{th} = \frac{\varkappa_1}{\varkappa_2 + T} + \varkappa_3 T^3 \qquad (7)$$

given by solid state physics.
Hence follows ⟨21⟩

$$k_{th}(T) = \frac{41,2}{T+4,9} + 6,55 \cdot 10^{-13} T^3 \pm 7\ \% \left(\frac{W}{cm\,^oC}\right) \qquad (8)$$

$$T \text{ in } {}^oK \qquad 900\,{}^oK \leq T \leq 3000\,{}^oK$$

On the base of the deviations of the several authors' results an error of k_{th} of $\pm$ 7 % can be considered as realistic.

In fig. 2 the thermal conductivity is represented graphically as a function of temperature with the porosity as parameter. The decreasing drop of the thermal conductivity with growing porosity can be seen.

2.2.3. Calculation of the temperature volumes

According to the burnup model formulated in chapter 2.1. there are three temperature zones in the fuel, the volumes of which are necessary for the calculation of the maximum burnup. The thermal consequences of the porosity migration towards the fuel axis in the plastic region - that is for temperatures above $T_{pl} = 1700\,{}^oC$ - is taken into account. This porosity migration creates a central channel and densifies the plastic fuel. This effect is characterized by a two zone porosity model ⟨21, 22⟩. Thus the following model is applied:

Fig. 3 : Radial cross section of the fuel model

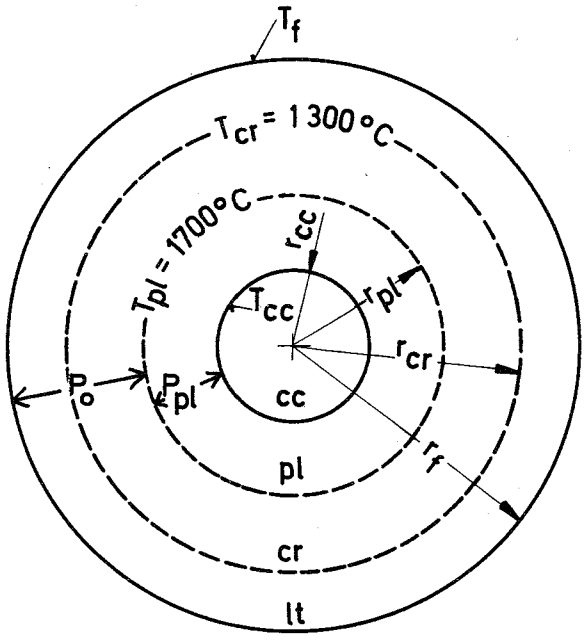

Indices:

cc = central channel
pl = plastic zone
cr = creep zone
lt = low temperature zone
f = fuel (-surface)

Symbols:

r_f = fuel radius
r_{cr} = radius of the creep-zone
r_{pl} = radius of the plastic-zone
r_{cc} = central channel radius

$T_f = T(r_f)$
$T_{cr} = T(r_{cr}) = 1300^{o}C$
$T_{cc}^{pl} = T(r_{cc}^{pl}) = 1700^{o}C$
T_{max}

Derived from the heat balance equation and the Fouriers' law of the proportionality of heat flux density and thermal gradient for radial heat flow the following relations for the ratios of the sectional area result

$$\frac{r_f^2 - r_{cr}^2}{r_f^2} = \frac{4\pi}{\chi} \int_{T_f}^{T_{cr}} k\,dT \qquad (9)$$

$$\frac{r_{cr}^2 - r_{pl}^2}{r_f^2} = \frac{4\pi}{\chi} \int_{T_{cr}}^{T_{pl}} k\,dT \qquad (10)$$

Substituting (5) and (7) in (9) and (10) the corresponding ratios of the axial volume elements are obtained.

$$\frac{V_{lt}}{V_f} = \frac{4\pi}{\chi}(1 - P_o^{\frac{2}{3}})\left[\varkappa_1 \ln\left(\frac{\varkappa_2 + T_{cr}}{\varkappa_2 + T_f}\right) + \frac{\varkappa_3}{4}(T_{cr}^4 - T_f^4)\right] \qquad (11)$$

$$\frac{V_{cr}}{V_f} = \frac{4\pi}{\chi}(1 - P_o^{\frac{2}{3}})\left[\varkappa_1 \ln\left(\frac{\varkappa_2 + T_{pl}}{\varkappa_2 + T_{cr}}\right) + \frac{\varkappa_3}{4}(T_{pl}^4 - T_{cr}^4)\right] \qquad (12)$$

$$\frac{V_{pl}}{V_f} = 1 - \frac{V_{lt}}{V_f} - \frac{V_{cr}}{V_f} \qquad (13)$$

A common constant availability factor G_{pl} is used for the densified plastic region and for the central channel. In the region for temperatures above $T_{pl} = 1700^{o}C$ there is only a dislocation of the fuel volume so that the volume of the theoretical dense fuel does not change. Therefore we can take the original not densified plastic volume V_{pl} in equation (1), so that the porosity migration has no influence on the volume ratios above.

2.2.4. Calculation of the hot gap volume and the central temperature

From some irradiation experiments the heat transfer coefficient fuel-cladding during operation time was found to be

$$h_{hg} = 1{,}1 \frac{W}{cm^2 {}^{o}C} \qquad (14)$$

In spite of uncertainties according to this value and its change during operation time this value is taken constant. It follows from an analysis of this value ⟨2, 23⟩ that there exists a partial contact of the fuel with the cladding so that during operation time a defined gap width is not given. Furthermore it is known from irradiation experiments that the fuel is cracked partially. That means that the original gap volume after having changed by thermal expansion of fuel and cladding is localized in cracks, too. To calculate the maximum burnup according to (1), it is irrelevant where the hot gap volume V_{hg} is localized.

In the following we consider an axial fuel volume element and calculate the increase of volume in radial direction. The porosity is fixed constant. The fuel can be regarded to be free of thermal stresses. In the plastic region

the thermal stresses are relaxed, in the brittle region the thermal stresses have caused the cracks. Therefore we can proceed as follows: The initial ring element $2\pi r_o dr_o$ is put plastically and incompressible around the circle with radius r given by thermal expansion of the region with radius r_o. There it expands according to the thermal expansion coefficient α from the constant initial temperature T_o to the temperature T(r).

The following differential equation is the result:

$$2\pi r dr - 2\pi r_o dr_o = 2\pi r_o dr_o 2 \int_{T_o}^{T(r)} \alpha(T) dT \qquad (15)$$

We integrate (15) over the fuel radius r_f for the following assumptions:

a) $\alpha_f = \alpha_1 T + \alpha_2$ T in ^oC

whereby $\alpha_1 = 3{,}9\ 10^{-9} \frac{1}{^oC^2}$ $\alpha_2 = 7{,}87\ 10^{-6} \frac{1}{^oC}$ ⟨24⟩

b) Parabolic temperature distribution which does not change during thermal expansion (that is constant thermal conductivity, constant heat source density and no central channel)

$$T(r) = T(r_o) = T_{cc} - \frac{\chi}{4\pi k} \frac{r^2}{r_f^2}$$

c) $T_o = 0^oC$

The following relative radial volume increase of the axial volume element is obtained

$$\frac{\Delta V_f}{V_f} = \alpha_2(T_{cc} + T_f) + \alpha_1 T_{cc} T_f + \frac{\alpha_1}{3} (T_{cc} - T_f)^2 \qquad (16)$$

For the relative hot gap volume results at last:

$$\frac{V_{hg}}{V_f} = 2\frac{\delta}{r_f} - \alpha_2(T_{cc}+T_f) - \alpha_1 T_{cc} T_f - \frac{\alpha_1}{3} (T_{cc}-T_f)^2 + 2\alpha_{sh} T_{sh} \qquad (17)$$

δ = initial gap width

α_{sh} = thermal expansion coefficient of cladding

T_{sh} = radial averaged cladding temperature

The fuel surface temperature T_f is essentially given by the heat transfer coefficient (14).

For the calculation of the fuel central temperature two cases must be distinguished:

a) $T_{cc} \leq T_{pl}$

that means that we get a solid cylinder with homogeneous porosity distribution. The wellknown relation

$$\chi = 4\pi \int_{T_f}^{T_{cc}} k\,dT \qquad \text{is valid}$$

respectively with (5) and (7) (18)

$$\varkappa_1 \ln \frac{\varkappa_2 + T_{cc}}{\varkappa_2 + T_f} + \frac{\varkappa_3}{4}\left(T_{cc}^4 - T_f^4\right) = \frac{\chi}{4\pi\left(1 - P_o^{\frac{1}{3}}\right)}$$

b) $T_{cc} \geq T_{pl}$

that means we get a hollow cylinder with a two zone porosity distribution. In (21) was derived the following relation

$$\int_{T_f}^{T_{cc}} k_{th}\,dT = \frac{\chi}{4\pi D_s\left(1+\frac{\delta}{r_f}\right)^2}\left\{\frac{1-P_{pl}}{1-P_{pl}^{\frac{2}{3}}}\left[\left(\frac{r_{pl}}{r_f}\right)^2 - \left(\frac{r_{cc}}{r_f}\right)^2 - 2\left(\frac{r_{cc}}{r_f}\right)^2 \ln\frac{r_{pl}}{r_{cc}}\right] + \right. \tag{19}$$

$$\left. + \frac{1-P_o}{1-P_o^{\frac{2}{3}}}\left[1 - \left(\frac{r_{pl}}{r_f}\right)^2 + 2\left(\frac{D_s\left(1+\frac{\delta}{r_f}\right)^2}{1-P_o} - 1\right)\ln\frac{r_f}{r_{pl}}\right]\right\}$$

D_s = relative smear density

With the condition, that the central channel is provided by the porosity of the plastic region related to the smear density, that no gap is present and with (7), (11), (12) and (13) we obtain.

$$\varkappa_1 \ln\left(\frac{\varkappa_2+T_{cc}}{\varkappa_2+T_{pl}}\right)+\left(\frac{\varkappa_3}{4}(T_{cc}^{\,4}-T_{pl}^{\,4}\right) = \frac{\chi}{4\pi}\,\frac{1}{1-P_{pl}^{\frac{2}{3}}}\,\frac{V_{pl}}{V_f}\left[1+\left(\frac{1-P_{pl}}{D_s}-1\right)\ln\left(1-\frac{D_s}{1-P_{pl}}\right)\right] \quad (20)$$

2.3. Argumentation of the swelling behaviour

2.3.1. Swelling rates

Though integral swelling rates for a wide temperature range are known from literature, some detailed indications on gas- and solid swelling rates have supported the application of zone specific swelling rates ⟨25, 26, 2⟩. Solid swelling rates between 0.3 and 1.25 v/o/10 000 $\frac{\text{MWd}}{\text{t heavy atoms}}$ depending on the degree of consumption of fissioned atom vacancy were published in ⟨25⟩. Gas swelling rate values between 0.55 and 0.8 v/o/10 000 $\frac{\text{MWd}}{\text{t heavy atoms}}$ dependent on used models were published in ⟨26, 27⟩. In addition we calculated such swelling rates. Swelling rates of both types were coordinated to the temperature zones by estimate in the following way. Regarding to the solid swelling rate the lattice vacancy of fissioned atoms will be widely consumed by the fission products at higher temperatures. At lower temperatures a smaller extent of lattice volume should be applicable because of lattice rigidity. Concerning the estimation of the gas swelling rate published results on fission gas release ⟨28, 29⟩ were taken into account. Furthermore the results of some calculations were included basing on following ideas:

Post irradiation examinations of high burnup specimens indicate that a certain amount of porous volume is existing at any time though remarkable external swelling has occured. These pores are non-growing and static gas pores as well as pores which are still under growth and migration.

Because of the uncertainty of data and models, which do not allow a quantitative classification of pores at present, a temperature, burnup and fission rate dependent amount of pores which is under remarkable high internal gas pressure is estimated as stabilized. They are of very small size ⟨27⟩, 10^{-5} to 10^{-6} cm in radius, if unmovable at medium or low temperatures. The main part of non-released fission gas seems to be trapped in such pores and in interstitial lattice positions. Hence the applied fission gas swelling rates could only be developed including fission gas release data.

The following swelling rates are resulting:

Table 1 : Applied swelling rates for the temperature zones

	low temp. zone 1300°C	creep zone 1300 - 1700°C	plastic zone 1700°C
Solid swelling rate	1	0,7	0,5
Gas swelling rate	0,6	1,0	0,2
Total swelling rate	1,6	1,7	0,7

The given swelling rate values are measured in v/o/10 000 $\frac{\text{MWd}}{\text{t heavy atoms}}$

2.3.2. Availability Factors

The amount of void volume within the fuel which can be filled by the swelling process in practical case will not be completely consumable. Resulting from publications ⟨30⟩ fuel plasticity is dependent on fission influence. Even after fuel is under compression by fuel clad interaction voids of high resistance geometry will remain. Many postirradiation examination results show this. To be understood as averaged over the operation time, corresponding to burnup of 8 or 10 %, we apply factors which are representing the availability of voids related to as-fabricated porous volume, but not saying a not available void only can be of as-fabricated nature.

We get by estimate the following availability factors:

Table 2 : Applied availability factors for the temperature zones

	low temp. zone 1300°C	creep zone 1300 - 1700°C	plastic zone 1700°C
availability factors	0,3	0,5	0,8

These assumptions may be working pessimistic when applied; from design reasons this is intention. The influence of their eventual variation will be discussed later in chapter 3.3.2.

2.4. Qualitative discussion of the fuel-cladding interaction

The burnup model, formulated in chapter 2.1., assumes that the resulting maximum burnup will not be influenced by the mechanical fuel-cladding interaction. Furthermore we assume for the calculations in chapter 3, that the radial and axial deformations of the cladding are relatively small and that there is no axial swelling of the fuel. These boundary conditions require a special interaction behaviour. This comprehensive interaction problem, which still is unsolved, is only touched in this work.

2.4.1. Multiaxial stress and strain analysis of the creeping sheath

To initiate the treatment of the interaction problem multiaxial stress and strain analysis of the creeping sheath was carried out.

If a symmetry of revolution and a plane state of strain is presumed the following equilibrium equation results:

$$\frac{d\sigma_r}{dr} + \frac{\sigma_r - \sigma_\theta}{r} = 0 \qquad (21)$$

Index r, Θ, z indicate the radial, tangential and axial component of the stress σ and the strain ε

and the following compatibility equations:

$$\varepsilon_r = \frac{du}{dr} \qquad \varepsilon = \frac{u}{r} \qquad \varepsilon_z = \text{constant} \qquad (22)$$

ε = (total) strain

u = radial deformation

Furthermore the following stress and strain relations were taken as a basis:

$$\begin{aligned}
\varepsilon_r &= \frac{1}{E_{sh}}\left[\sigma_r - \mu_{sh}(\sigma_\theta + \sigma_z)\right] + \alpha_{sh} T_{sh} + \varepsilon_{rc} \\
\varepsilon_\theta &= \frac{1}{E_{sh}}\left[\sigma_\theta - \mu_{sh}(\sigma_r + \sigma_z)\right] + \alpha_{sh} T_{sh} + \varepsilon_{\theta c} \qquad (23) \\
\varepsilon_z &= \frac{1}{E_{sh}}\left[\sigma_z - \mu_{sh}(\sigma_z + \sigma_\theta)\right] + \alpha_{sh} T_{sh} + \varepsilon_{zc}
\end{aligned}$$

E_{sh} = Young modulus of the sheath
μ_{sh} = Poission ratio of the sheath

ε_r, ε_θ, ε_z are the components of the total strains - ε_{rc}, $\varepsilon_{\theta c}$, ε_{zc} are the components of the strains due to the creeping.

The strains, given by the equations above, are distributed in elastic, thermal expansion and creep increments.

The stress and strain state of the sheath were determined by the following iterative method ⟨31⟩ . Thereby is given the inner and outer pressure, the axial force, the temperature distribution and the creep law in the form of the Norton's creep law

$$\dot{\varepsilon}_{sh} = K\sigma^n \qquad (24)$$

$\dot{\varepsilon}_{sh}$ = Creep rate of the sheath
K,n = constants relating to the Norton's creep law

These input data respectively functions can be dependant on time. For the time t = 0, the creep strains are $\varepsilon_{rc} = \varepsilon_{\theta c} = \varepsilon_{zc} = 0$. The stresses and strains are calculated with (21), (22) and (23). From the components of the stress an equivalent stress is determined on the base of the von Mises theory and using the Norton creep relation (24), an equivalent creep strain is calculated for the following time interval. This creep strain is distributed in the three directions by the help of the von Mises theory. The creep strain components soobtained are now used as input functions of (23), so that new strain and stress values can now be calculated and the procedure begins again.

2.4.2. Axial expansion of the fuel

The three dimensional fuel swelling can both fill internal void volumes and occur externally in radial and axial direction. The internal void volume is essentially given by the hot smear density and the porosity availability factors. The external swelling is determined by external restraints and by the fuel-cladding interaction. There are only allowed small radial cladding deformations from reasons of coolant channel cross sections and brittleness of the cladding material.

The axial swelling has relevant consequences on the maximum operation time, e.g. an axial expansion of 4 v/o causes a rise of the maximum operation time of 25 % (fig. 6). Therefore the question arises by which factors the axial tolerances are limited. On the one hand this tolerance is given essentially by safety considerations. These must be oriented - the Na2-core ⟨32⟩, which is taken as basis for all following calculations - on two values: Firstly, a change of the fuel length of 1 cm at a fuel-length of 100 cm, corresponding to an averaged value of thermal expansion causes about 2 $ reactivity change in the core. Secondly, a temporal reactivity change of 2.5 $/s is regarded as the maximum allowable limit for the core. Considering a sudden return movement of the axially expanded state to the original length, for which reasons ever, we see, that this allowed length change will mainly be consumed by thermal expansion. Therefore an axial swelling cannot be allowed in our calculations according to Na2. Apart from the fact, that this case is extremely pessimistic, the axial thermal expansion can be reduced by using dished pellets. On the other hand the long friction area could cause a not allowed axial deformation of the sheath, because of the interaction fuel cladding, if no axial restraint would be applied.

2.4.3. Rough estimate of the swelling pressure of the fuel

In the following an estimate of the swelling pressure of the fuel is made for strongly simplified assumptions. We consider the fuel swelling against the cladding which is assumed to be rigid. Then the radial fuel swelling velocity directed to the outside is equal to the creep rate of the fuel directed to the axis. According to the creep law, valid for the fuel, an annular tension σ is induced in a ring with radius r and the width dr. Corresponding to the pressure formula for thin walled tubes.

$$dp_{sw} = \sigma \frac{dr}{r} \qquad (25)$$

p_{sw} = swelling pressure
σ = stress

a differential of the swelling pressure is resulting. The total swelling pressure is obtained by integration of (25) over the radius r. The pressure formula is only valid for thin walled tubes. But from the equality of (26)

and (27) results a strong drop of the stress with rising temperature, so that this integration is justified.

The radial swelling velocity of the fuel is connected with the swelling rate under the assumption of a constant isotropic fuel swelling in the following way:

$$s = \frac{1}{3} \frac{A}{t} \cdot S \qquad (26)$$

$s = \frac{1}{t} \frac{\Delta L}{L_{th}}$ = (linear) swelling velocity

t = time

The ratio burnup divided by time A/t is given by (2) and proportional besides other factors to the linear rod power

The creep rate $\dot{\varepsilon}_f$ of the fuel is given by the publications of several authors ⟨33 to 36⟩. These results can be represented in the following form according to ⟨36⟩.

$$\dot{\varepsilon}_f = e^{-\frac{Q}{RT}} (\omega_1 \sigma + \omega_2 \sigma^{\omega_3}) \qquad (27)$$

Q = activation energy

ω_1, ω_2, ω_3 = constants relating to the creep law of the fuel

R = gas constant

(26) and (27) is equalized and this equation is solved with respect to the stress σ. Then σ is substituted in (25) and the swelling pressure is obtained in dependance of the temperature distribution by integration of (25).

In the following the swelling pressure is estimated in an optimistic and pessimistic way. These estimations are represented in fig. 4. For the pessimistic estimate the experimental data of Armstrong ⟨34⟩ for stoichiometric UO_2 were used as the basis. $\omega_1 = 7.26 \times 10^6$ cm^{2}kp^{-1}h^{-1}, $\omega_2 = 2.22 \times 10^{-2}$ cm^{2}kp^{-1}h^{-1}; $Q = 91$ kcal/mol, $\omega_3 = 4$. For the ranges of temperature and rod power of interest we obtain swelling pressures of 20 to 3×10^3 kp/cm^2. According to this estimate, practically all zones of the Na2-core must be regarded as being imperiled, if it is assumed that the cladding, in addition to the fission gas pressure has to sustain about 100 kp/cm^2 swelling pressure.

For the optimistic estimate we use the creep data for $UO_{2.04}$ measured in ⟨35⟩. $\omega_1 = 1700\ cm^2/kph^{-1}$, $\omega_2 = 5 \cdot 10^{-6}\ cm^{2-1}kph^{-1}$, $Q = 56$ kcal/mol, $\omega_3 = 4$. With these data we obtain swelling pressures between 0.3 and 200 kp/cm^2 for the range of interest, and thus practically no zone in the Na2-core would have to be regarded as imperiled under the above assumption.

Even the creep analysis of irradiated specimens ⟨30⟩ do not allow accurate quantitative statements. However, according to these results the creep strength under irradiation decreases by some powers of ten (thermal spikes, increase in point defect concentration) so that the swelling pressure load on the cladding remains negligibly small in any case.

One comes to the conclusion that an estimate of the swelling pressure does not lead at present to satisfactory results. Furthermore it is not possible at present, to obtain a design criterion regarding to the maximum operation time on the base of the mechanical interaction fuel clad.

3. Maximum operation time computer analysis of the Na2-Core

3.1. General aspects concerning the dependences of the maximum operation time on core position and parameters

Parameter classification

The essential dependences of the maximum operation time on parameters are clearly represented in fig. 5 on the basis of (1) and (2).

Two types of parameters can be distinguished:

I. Parameters, which directly influence the maximum operation time
   a) the fuel radius r_f, given by the outer radius of the sheath, the initial gap width δ and the sheath thickness d_{sh}
   b) the swelling rates S_{lt}, S_{cr} and S_{pl}
   c) the availability factors G_{lt}, G_{cr} and G_{pl}
   d) the initial porosity P_o
   e) the linear rod power χ

II. Parameters, which indirectly influence the maximum operation time over the volumes V_{lt}, V_{cr}, V_{pl} and V_{hg} given by the radial temperature distribution

a) the coolant temperature T_{Na}, given by the sodium inlet and outlet temperature and the linear rod power distribution
b) the heat transfer coefficient fuel clad h_{hg}
c) the zone boundary temperatures T_{cr} and T_{pl}
d) the porosity of the densified plastic zone P_{pl} and the central channel radius r_{cc}
e) the initial gap width δ
f) the thermal expansion coefficients of the fuel α_f and the sheath α_{sh}
g) the thermal conductivity of the theoretical dense fuel K_{th}
h) the initial porosity P_o
i) the linear rod power

The linear rod power and the initial porosity influence the maximum operation time both directly and indirectly over the radial temperature distribution.

The maximum burnup respectively the maximum operation time is only dependant on the core position with regard to the linear rod power and the coolant temperature.

One zone model

In the following we generally analyse the dependence of the maximum operation time on the core position. The clearest case is present, if the swelling rates and the availability factors in the three zones are equal, that means if it is realized a one zone model.

For the case of a one zone model it results from (1)

$$A_{max} = \frac{P_o G + X}{(1-P_o)S} \tag{28}$$

whereby

$G = G_{lt} = G_{cr} = G_{pl}$ = availability factor for the one zone model

$S = S_{lt} = S_{cr} = S_{pl}$ = swelling rate for the one zone model

$X = \frac{V_{hg} + V_{ax}}{V_f}$ = relative hot gap and axial expansion volume ratio

As explained in chapter 2.4.2. we use $V_{ax} = 0$ for our calculations. From the computer calculation for the Na2-core treated in the following chapter results that V_{hg}/V only changesabout ~20 % within the core. Because $X = V_{hg}/V$ is about 50 % of $P_o G$, the maximum burnup A_{max} can be regarded as constant in a first approach. According to (2) the maximum operation time is given by a $\frac{1}{\chi}$ - core position dependance. In fig. 6 A_{max} is represented graphically as a function of the relative fuel density $D_f = 1 - P_o$ with swelling rate, availability factor and relative hot gap and axial expansion volume ratio as parameters. The sensitive influence of these parameters on the maximum burnup can be seen. To make clear this sensitive parameter dependance the total differential of (28) is formed. With respect to $X \ll G$, it results

$$dA_{max} = -\frac{G}{S\,D_f^2}\,dD_f + \frac{1}{S}\left(\frac{1}{D_f} - 1\right)dG - \frac{(1-D_f)G+X}{D_f S^2}\,dS + \frac{1}{S\,D_f}\,dX \qquad (29)$$

For the averaged values used in fig. 6

$$D_f = 0{,}85 \qquad G = 0{,}5 \qquad X = 0{,}05 \qquad S = 1{,}6\cdot 10^{-6}\ \frac{t}{MWd}$$

results from (29) that a burnup of 9360 MWd/t (heavy elements) corresponding to 1 % of heavy atoms is caused by the following parameter changes

$$dA_{max} = 9360\ \frac{MWd}{t} \qquad \begin{cases} dD_f = -0{,}022 \\ dG = 0{,}086 \\ dX = 0{,}013 \\ dS = -0{,}163 \cdot 10^{-6}\ \frac{t}{MWd} \end{cases}$$

Three zone model

If the swelling rates and availability factors in the three zones are not constant, the $\frac{1}{\chi}$ - dependance of the maximum operation time is deformed by the core position dependance of the volumes V_{lt}, V_{cr}, V_{pl} and V_{hg} given by the temperature distribution.

It is possible to fix the following general statements. The burnup required to fill the available porous volume of a zone by its swelling is obtained by a simple consideration as follows

$$A_i = \frac{P_o}{1 - P_o}\,\frac{G_i}{S_i} \qquad i = lt,\ cr,\ pl \qquad (30)$$

Equat.30 shows that the ratio G/S of the concerning zone determines its maximum burnup.

The burnup necessary to fill the hot gap volume by simultaneous swelling of the three zones is given by

$$A_{hg} = \frac{V_{hg}}{(1-P_o)(S_{1t}V_{1t}+S_{cr}V_{cr}+S_{pl}V_{pl})} \qquad (31)$$

This is valid because of the assumed free displaceability of the fuel.

Three cases can easily be overlooked:

a) $\frac{G_1}{S_1} > \frac{G_2}{S_2} > \frac{G_3}{S_3}$ 1 = pl, cr or 1t; 2, 3 complementary

and max of $A_i > A_{hg}$

In this case the zone with the biggest value of $\frac{G_i}{S_i}$ determines the picture if this zone has a relatively big volume

b) $\frac{G_{pl}}{S_{pl}} \simeq \frac{G_{cr}}{S_{cr}} \simeq \frac{G_{1t}}{S_{1t}}$

That means that the single axial zone elements are filled by themselves in nearly the same time. Regarding the remaining filling of the hot gap volume the zone with the biggest swelling rate determines the picture if this zone has a relatively big volume.

c) $A_{hg} >$ max of A_i

This is surely fulfilled if $V_{hg} > P_o V_f$. Here like case b) the zone with the biggest swelling rate determines the picture if this zone has a relatively big volume.

As it can be seen in chapter 3.3.1. case a) is realized for our data and conditions.

3.2. Computer listing of the maximum operation times for the Na2-core

In table 3 the input data for the computer program are compiled〈37〉 These data are composed of the material data discussed in chapter 2 and the required Na2-data〈32〉. The computer listing is represented in fig. 7. From left to

right the core radius is given and from above to below the axial core height. Relating to this diagram the sodium flows from above to below. In this two dimensional diagram the values represent the maximum operation times for the concerning radial and axial core positions. Instead of this two dimensional representation a curved area of the lifetimes extending over the R-Z-plane would be very clear.

As the Na-2 core is chaped like a vertical cylinder and since the distribution of fission rates and the temperature are in rotational symmetry to the cylinder axis, it is sufficient to know the lifetimes for the rotational area. The rotational area is formed by the core height of 96 cm and the core radius of 77 cm. Radially, the core is subdivided into two fuel zones of different degrees of enrichment. The fuel zones can be subdivided into idealized annular subassembly (four on the inside, two on the outside).

For better clarity, the axial lifetime profiles for 5 radial positions, a line connecting the points of minimum lifetime and lines of equal lifetime (450 d, 500 d) where plotted in the computer listing.

The axial lifetime profiles exhibit a relatively flat curve over a wide internal core range. However the boundary zones (mantle, top and bottom regions) clearly exhibit increasing lifetimes. Quantitively, for the fraction of the core volume with lifetimes longer than 500 d, the resultsis some 40 vol.% (zone I 25 vol.%, zone II 60 vol.%).

The minimum line indicates the points of the minima of the axial lifetime profiles. The slightly curved decreasing slope of the minimum line can be seen. The absolute minimum localized at (R,Z) = (9, 56), amounts to 397 d. With increasing distance from the center axis of the core the values of the minimum line increase only a little i.e. about (+ 7 %). Only at the very edge of the core $R \geq 74$ cm there is a steep increase which is proportional to the radial power decrease in this core area, because there exists only one zone, so that the influence of the temperature distribution is negligible.

In the inner core region the subassembly effect becomes valid. This is evident from the lines of equal lifetimes which show a little jump at the boundary between subassemblies. Subassembly effect, in our terminology,

means the effect that a constant throughput of coolant within one subassembly results in a temperature jump of the coolant between two adjacent subassemblies as a consequence of the radial power gradient. It does not appear at all points where the maximum temperature is smaller than 1300°C, so that only one zone is existing.

In fig. 8 the maximum burnup is represented in dependance on smear density with linear rod power and cladding temperature as parameters on the base of the required data, compiled in fig. 7. This picture shows the influence of the temperature distribution on the maximum burnup if a three zone model is used.

3.3. Discussion of the results

3.3.1. Parameter analysis

In this chapter the results of the computer listing are discussed especially the axial lifetime profiles and the minimum line on the base of the given data with the help of the considerations of chapter 3.1.

Chapter 3.1. shows that in the case of a three zone model the maximum operation times are relevantly dependant on the ratios G_i/S_i. In table 4 these ratios and the corresponding burnups required to fill the single zones are represented. Furthermore the burnup required to fill the hot gap volume by simultaneous swelling of the fuel zones according to (31) is included.

Table 4 : Applied ratios $\frac{G_i}{S_i}$ and corresponding burnups A_i and A_{hg}

$$\left[P_o = 0{,}155 / \frac{V_{hg}}{V_f} = 0{,}045/\overline{S} \quad = 1{,}4 \cdot 10^{-6} \frac{t}{MWd} \right]$$

zone i	G_i	$B_i \left[10^{-6} \frac{t}{MWd}\right]$	$\frac{G_i}{S_i} \left[10^{6} \frac{MWd}{t}\right]$	$A_i \left[10^{4} \frac{MWd}{t}\right]$
pl	0,8	0,7	1,14	20,9
cr	0,5	1,7	0,29	5,5
lt	0,3	1,6	0,19	3,5
hg	-	-	-	3,8

It results that A_{pl} is relevantly bigger than A_{cr} and A_{lt} as well as A_{hg}. Consequently the case a) of chapter 3.1. is realized so that the plastic region is prevailing if its volume is comparable with the low temperature and creep zone volume.

In fig. 9b the axial dependance of the temperature volume ratiosand the resulting axial lifetime profile is represented for a position near the core axis. The axial profile of the volume ratios can be understood with the help of the equations (11), (12), (13). If the maximum temperature is smaller than $T_{cr} = 1300^{o}C$, there is only one temperature zone. If the maximum temperature is bigger than $1300^{o}C$ and smaller than $1700^{o}C$ a two zone model is realized. $\frac{V_{lt}}{V_f}$ is approximately proportional to $\frac{1}{\chi}$. This is shown in fig. 9 for a cosine shaped power curve. $\frac{V_{cr}}{V_f}$ is then complementary to 1. If the maximum temperature is bigger than $T_{pl} = 1700^{o}C$ a three zone model is realized. There is no change relating to the axial profile of $\frac{V_{lt}}{V_f}$ but $\frac{V_{cr}}{V_f}$ is now exactly proportional to $\frac{1}{\chi}$. $\frac{V_{pl}}{V_f}$ is complementary to 1. In all cases the nonsymmetric curve of the sodium temperature relating to the central plane must be regarded. Therefore the low temperature volumes are relatively bigger in the colder half of the core for positions axialsymmetric to the central plane.

Fig. 9a shows that in the outer regions the $\frac{1}{\chi}$ - dependance is realized according to the one zone model if the maximum temperature is lower than $1300^{o}C$. This curve is only deformed a bit if the creep zone is existent because of the relatively small differences of the G/S ratios. A relevant flattening of the lifetime profile occurs if the plastic zone is existent due to the approximately contrary effects of linear rod power and the plastic volume.

The position of the minimum of the lifetime coincides with the onset of the plastic zone in the colder half of the core, because the plastic zone has a smaller axial extension measured from central plane in this core half than in the hotter one. In fig. 9a the thin drawn line representates the one zone model if the datas of the low temperature zone are used. The closely dotted line corresponds with a two zone model whereby the low temperature zone data are attributed to the plastic zone, too. The thick line representates completely the three zone model.

Fig. 10 shows how the shape of the axial lifetime profiles is strongly influenced by the grading of the swelling rates and availability factors among each other.

The conclusion can be drawn that if the ratios $\frac{G_i}{S_i}$ are fixed an increase of the lifetime is either possible by a decrease of the plasticity temperature T_{pl} or by an increase of the temperature profile An increase of the temperature profile can be reached by a higher sodium temperature, a smaller hot gap heat transfer coefficient and a smaller thermal conductivity of the theoretical dense fuel. The effect of the fuel porosity and the linear rod power which influence the maximum operation time both directly and indirectly over the temperature distribution is calculated in the following chapter. This increase of lifetime is connected with a shifting of the position of the minimum of the axial lifetime profile in direction of the sodium inlet because this position is given by the onset of the plastic zone. The value of this minimum lifetime is naturally independant on the swelling rate and availability factor of the plastic zone.

Furthermore the lifetime diagram is relevantly influenced by variations of availability factor G and swelling rate S, especially of the ratios $\frac{G}{S}$ among each other. These effects are calculated in the following chapter.

3.3.2. Error analysis

Table 5 indicates the influence of the errors of the important parameters. The errors were evaluated by the reactor design and by irradiation experiments. Lifetime diagrams were calculated for the input data represented in table 3 and the following parameter variations.

α) linear rod power and initial fuel porosity, which influence the maximum operation time both directly and indirectly over the temperature distribution.

ß) the swelling rates and the availability factors of the three zones whereby the grading of these parameters between each other are kept approximately constant.

γ) fuel thermal conductivity, heat transfer coefficient fuel clad, zone boundary temperatures and sodium temperature increase which influence the maximum operation time only indirectly over the temperature distribution.

A part of the computer listings is represented at fig. 11 to fig. 15. The computer diagrams are described in table 5 by the following three values:

a) value and position of the absolute minimum of the lifetime
b) shift of the minimum line (in the direction of the center of the core (+), in the direction of coolant inlet (-).
c) position and value of the minimum lifetime in the center plane of the core

The following results are obtained:

a) The absolute minimum of the lifetime is not influenced by the range of variation of the swelling rate and the availability factor of the plastic zone. The influence remains relatively small with the parameters of rod power and sodium temperature increase. The absolute minimum of the lifetime reacts very sensitive to the two parameters of fuel porosity and swelling rate in the low temperature range. The influence of the heat transfer coefficient fuel clad remains relatively small.
b) As we have seen in the preceding chapter the absolute minimum of the lifetime is located at the onset of the plastic zone in the colder half of the core because the ratio $\frac{G}{S}$ is relevantly larger in the plastic zone than in the outer zones. Therefore the availability factors, the swelling rates and the creep temperature (1300°C) have no influence on this position. The parameters which influence the temperature distribution cause a shifting of the minimum line, only the effect of the sodium temperature increase is negligible because the minimum line is located at the colder half of the core.
c) The minimum of the lifetime in the core center plane is at the edge of the core, with one exception, and it is about 10 % higher than the absolute minimum, which must always be sought near the core axis.

The algebraic sum of all the single errors shown in table 5 is $^{+48,2\%}_{-58,1\%}$ for the absolute minimum of lifetime. However, if all the pessimistic and optimistic values (with respect to the lifetime) are fed into the program simultaneously the devation from the standard value for the absolute minimum of the lifetime is $^{+66\%}_{-36\%}$. As estimates of this type are not very realistic, the mean square error $\sqrt{\Sigma_{i=1}^{n} \Delta x_i^2}$ for the single errors Δx_i shown in table 5 is calculated to be ± 20 %.

4. Summary

The aim of this work was the calculation and analysis of the maximum operation time respectively of the maximum burnup of the fuel pins of a core as a function of the distance from the core centerline and core mid-plane.

As the basis of this examination there was taken a defined three zone volume balance relating to the swelling of the fuel volume and the consumption of void volume, given by the hot gap volume, the axial expansion and ratios of the pore volume. To calculate the maximum burnup with this model the radial temperature distribution had to be treated quantitatively. For doing this a new porosity relationship of the thermal conductivity was used, which was developed recently. Furthermore a two zone porosity model was applied for the characterization of the porosity migration in the plastic region connected with the central channel formation and a densification in the plastic region. ("Thermal central channel effect"). To get the hot gap volume it was necessary to calculate the radial thermal expansion of the fuel at fixed porosity on the base of a plastic behaviour. The applied swelling rates and availability factors were argued. The still unsolved fuel clad interaction problem was discussed. To initiate the quantitative treatment of the interaction problem a multiaxial stress and strain calculation of the creeping sheath was carried out by an iterative method. It was founded that no axial swelling was allowed and the swelling pressure of the fuel was roughly estimated.

After having discussed generally the dependance of the maximum operation time on core position and parameters the lifetime was calculated as a function of the position within the core for the case of the Na2-Core. We roughly got constant maximum operation times in radial direction, in axial direction we also have constant values in a wide range, but towards the core edge we have a strong rise of the maximum operation times. We made extensive parameter studies, to test the sensitivity of the maximum operation times with respect to the influence of temperature distribution, swelling rates , availability factors etc. This parameter study is especially important with respect to the grade of accuracy applied on fuel pin specific data like swelling rates, availability factors,

plastic and creep data, coefficients of the thermal conductivity equation , thermal expansion coefficients and heat transfer coefficients By this procedure we can check the range of the validity of the results and get a general survey on fuel pin behaviour under operational conditions.

Nomenclature

A	=	burnup
C	=	constants relating to pore conductivity
D	=	relative fuel density
d	=	length of pore in direction of heat flow, thickness
E	=	young modulus
G	=	availability factor
h	=	heat transfer coefficient
K	=	constant relating to Norton's creep law
k	=	thermal conductivity
L	=	length
n	=	constant relating to Norton's creep law
P	=	porosity
p	=	pressure
Q	=	activation energy
R	=	gas constant
r	=	radius
S	=	swelling rate
s	=	swelling velocity
T	=	temperature
t	=	time
u	=	radial deformation
V	=	volume
z	=	axial direction
α	=	thermal expansion coefficient
α_i	=	constants relating to thermal expansion
β	=	shape factor
δ	=	initial gap width
ε	=	strain
η	=	constant relating to linear porosity relation
θ	=	tangential
$\varkappa_i$	=	constants relating to thermal conductivity
μ	=	Poission ratio
ρ	=	(absolute) density

σ = stress

χ = linear rod power

ω_i = constants relating to creep law of UO_2

Indices

ax = axial

cc = central channel

cr = creep

cond = conduction

f = fuel, fuel surface

h = heavy elements

hg = hot gap

lt = low temperature

max = maximum

Na = coolant sodium

p = pore

pl = plastic

r = temperature radiation

s = smear

sh = sheath (cladding)

sw = swelling

th = theoretical

o = initial

1,2,3 = distinction of constants

Literature

(1) D. Geithoff, G. Karsten, K. Kummerer
Irradiation Performance of Fast Reactor Fuels - Proceedings of the 1967 Nuclear Metallurgy
Symposium - Scottsdale, Arizona, Nuclear Metallurgy, Vol. 13, p. 396

(2) H. Beißwenger, H. Blank et al.
The Development of Fuel Pins for Fast Breeder Reactors
KFK 700/Eur 3713 d - Contribution V - December 1967 (in German)

(3) H. Kämpf
The Porosity Dependance of Heat Conductivity of Ceramic Fuels
KFK-Report under preparation (in German)

(4) Ross, A.M.
The Dependence of the Thermal Conductivity of Uranium Dioxide on Density, Microstructure, Stoichiometry and Thermal-Neutron Irradiation
AECL-1096 (1960)

(5) J.A.L. Robertson, A.M. Ross, M.J.F. Notley and J.R. MacEwan
Temperature Distribution in UO_2-Fuel Elements
J. Nucl. Mat. 7, No. 3, 225 - 262 (1962)

(6) H. Mogard et al.
Fuel Development for Swedish Heavy Water Reactors
Geneva Conference, p. 608 (1964)

(7) M.J.F. Notley and J.R. MacEwan
The Effect of UO_2-Density on Fission Product Gas Release and Sheath Expansion - AECL-2230, March 1965

(8) J. Vogt, L. Grandell and M. Remfors
AB Atomenergi (Sweden) Int. Report RMB-527 (1964) cited by IAEA Panel on Thermal Conductivity in Uranium Dioxide, Vienna 1966
Techn. Report Series No. 59

(9) M.J.F. Notley and J.B. MacEwan
Nucl. Appl. 2 (1966) 117

(10) J.R. MacEwan, R.L. Stoute and M.J.F. Notley
Effect of Porosity on the Thermal Conductivity of UO_2
J. of Nucl. Mat. 24 (1967) 109 - 112

(11) A. Biancheria
The Effect of Porosity on Thermal Conductivity of Ceramic Bodies
Trans ANS 9, 1, 1966

(12) A. Biancheria
The Thermal Conductivity of Multiphase Ceramic Nuclear Fuels
Trans ANS 10, 1, 1967

(13) H. Fricke
A Mathematical Treatment of the Electric Conductivity and Capacity of Disperse Systems
Physical Review, 24, 1924

(14) J.A. Christensen
Uranium Dioxide Thermal Conductivity - Trans ANS 7, 2 - 1964

(15) J. Hetzler, E. Zebroski
Thermal Conductivity of Stoichiometric and Hypostoichiometric Uranium Oxide at High Temperatures - Trans ANS 7, 2 p. 392 (1964)

(16) H.E. Schmidt, unpublished

(17) D.M. Coplin et al.
In-Pile Direct Measurement of UO_2 Thermal Conductivity
Trans ANS 8, 1 (1965) 35

(18) W.E. Baily et al.
In-Pile Thermal Conductivity of UO_2 and 20/80 $(Pu/U)O_2$ Specimens
Trans ANS 8, 1 (1965) 39

(19) F.J. Hetzler et al.
Thermal Conductivity of 20/80 (Pu/U)O_2 - Trans ANS 8, 1 (1965) 36

(20) H.E. Schmidt, unpublished

(21) H. Kämpf
The Influence of inner Geometry on Temperature Distribution of Fast Reactor Fuel Pins - KFK 751 (EUR 3710 d), February 1968 (in German)

(22) E.G. Stevens
Derivation of a Sintering Correction Factor for Fast Oxide Fuels
Trans ANS 11, 1, 1968

(23) H. Kämpf
General gap-equation for the heat transfer fuel cladding in fuel pins with pellet fuel - KFK 604, June 1967 (in German)

(24) J. Roth et al.
Development and Testing of PuO_2-UO_2 Fast Reactor Fuels
Numec 2389 - 4 (1964) 35

(25) E.L. Zebroski et al.
Reviews of Status of Technology of Fast Reactor Fuels
ANS 101 (1967) p. 63 - 80

(26) BRT Frost, E. Wait
Irradiation Experiments on Plutonium Fuels for Fast Reactors
Symposium on the use of Plutonium as a Reactor Fuel - 1967 Brussels
SM 88/25

(27) F.A. Nichols
Behaviour of Gaseous Fission Products in Oxide Fuel Elements
WAPD - TM - 570

⟨28⟩ H. Lawton, K.Q. Bailey, E. Edmonds, H.E. Tilbe
The Irradiation Behaviour of Plutonium-Bearing Ceramic Fuel Pins
London Conference on Fast Breeder Reactors, May 1966, paper 4B/4

⟨29⟩ R.E. Skavdahl, C.V. Spalaris, E.L. Zebroski
U.S. Experience on Irradiation Performance of UO_2-PuO_2 Fast Reactor Fuel - Intern. Symp. on Plutonium Fuels Technology, Nucl. Met. Vol. 13

⟨30⟩ S.T. Konobeevsky
On the Nature of Radiation Damage in Fissile Materials
J. Nucl. Eng. 3, 336 - 365, 1956

⟨31⟩ S.S. Manson
Thermal Stress and Cycle fatigue
MacGraw Hill Book Company, New York 1966

⟨32⟩ K. Gast, G. Schlechtendahl
Fast Sodium Cooled Reactor Na2
KFK 660/EUR 3706 (Reference design, in German)

⟨33⟩ R. Scott et al.
The Plastic Deformation of Uranium Oxide above 800°C
Journal of Nuclear Materials, (1959), p. 39 - 48

⟨34⟩ W.M. Armstrong et al.
Creep Deformation of Stoichiometry - Uranium Dioxide
Journal of Nuclear Materials, 7, No. 2 (1962), p. 133 - 141

⟨35⟩ W.M. Armstrong, W.R. Irvine
Creep Deformation of Non-Stoichiometric Uranium Dioxide
Journal of Nuclear Materials 9, No. 2 (1963), p. 121 - 127

⟨36⟩ L.E. Poteat, C.S. Just
Grain Boundary Reactions During Deformations, ORNL-P-2371 (1966)

⟨37⟩ Fortran-Programm written von A. Wickenhäuser - Gesellschaft für Kernforschung

MATERIAL DATA:	
INITIAL GAP WIDTH	$\delta = 70\ \mu$
INITIAL POROSITY	$P_o = 0.155$
POROSITY IN THE PLASTIC ZONE	$P_{pl} = 0.05$
HEAT TRANSFER COEFF. FUEL-SHEATH	$h_{hg} = 1.1\ \frac{W}{cm^2\ °C}$
THEOR. THERM. CONDUCTIVITY FUEL	$K_{th,f} = (\frac{41.2}{T+4.9} + 6.55 \cdot 10^{-13}\ T^3)\ \frac{W}{cm\,°K}$
THERMAL CONDUCTIVITY SHEATH	$K_{sh} = 0.21\ \frac{W}{cm\ °C}$ T in °K
THERM. EXPANSION COEFF. FUEL	$\alpha_f = (3.9 \cdot 10^{-9}\ T + 7.87 \cdot 10^{-6})\ \frac{1}{°C}$
THERM. EXPANSION COEFF. SHEATH	$\alpha_{sh} = 1.75 \cdot 10^{-5}\ \frac{1}{°C}$ T in °C
CREEP TEMPERATURE	$T_{cr} = 1300\ °C$
PLASTIC TEMPERATURE	$T_{pl} = 1700\ °C$
SWELLING RATES	$S_{lt} = 1.6 \cdot 10^{-6}\ \frac{t}{MWd}$
FOR THE THREE	$S_{cr} = 1.7 \cdot 10^{-6}\ \frac{t}{MWd}$
TEMPERATURE ZONES	$S_{pl} = 0.7 \cdot 10^{-6}\ \frac{t}{MWd}$
AVAILABILITY FACTORS	$G_{lt} = 0.3$
FOR THE THREE	$G_{cr} = 0.5$
TEMPERATURE ZONES	$G_{pl} = 0.8$

REACTOR DATA:	
LINEAR ROD POWER	$X_{max} = 420\ W/cm$
Na INLET TEMPERATURE	$T_{Na,in} = 385\ °C$
Na OUTLET TEMPERATURE	$T_{Na,out} = 585\ °C$
HEAT TRANSFER COEFF. SHEATH - Na	$h_{Na} = 14\ \frac{W}{cm^2\ °C}$
OUTER SHEATH RADIUS	$r_{sh,out} = 0.3\ cm$
INNER SHEATH RADIUS	$r_{sh,in} = 0.262\ cm$
SMEAR DENSITY	$D_s = 0.80$
AXIAL SWELLING VOL.	$V_{ax} = 0$
CORE RADIUS	$R = 76.5\ cm$
CORE HEIGHT	$Z = 95\ cm$

MESH DATA:	
RADIAL STEP WIDTH	$\Delta R = 2.41\ cm$
NUMBER OF RADIAL POINTS	30
AXIAL STEP WIDTH	$\Delta Z = 2.0\ cm$
NUMBER OF AXIAL POINTS	49

TABLE 3 INPUT - DATA

Table 5: Error analysis of the maximum operation time

Parameter variation				Absolute minimum of the life time			Shifting of the min. line	Minimum of the lifetime in the central plane		
Parameter		normal value	Error	value (d)	position (R/Z)	deviat. (%)	(cm)	val. (d)	pos. R/Z	deviat. (%)
linear rod power , $\chi(R/Z)$ $(\frac{W}{cm})$			→ (+20%)	392	7/52	- 1,2	-8	453	7	+2,3
			→ (-20%)	413	7/70	+5	+14	441	33	-1
initial porosity P_o (1) ,			→ 0,175(+13%)	441	7/54	+11,7	-2	490	52	+12,4
		0,155	→ 0,135(-13%)	335	7/58	-15,6	+ 2	363	52	-16,6
swelling rates $S_i\left[v/o/10^4 \frac{MWd}{t(U+Pu)}\right]$	S_{pl}		→ 0,9(+28%)	395	12/56	0	-	433	52	-0,6
		0,7	→ 0,5(-28%)	395	12/56	0	-	438	52	+0,6
	S_{cr}		→ 1,9(+12%)	381	7/56	-3,5	-	419	52	-4
		1,7	→ 1,5(-12%)	411	9/56	+4	-	454	52	+4
	S_{lt}		→ 1,8(+13%)	364	7/56	-7,4	-	403	52	-7,6
		1,6	→ 1,4(-13%)	432	7/56	+9,4	-	473	52	+8,5
	$\max(S_{pl},S_{cr},S_{lt})$		→ 0,9;1,9;1,8	352	7/56	-10,9	-	387	52	-11,7
	$\min(S_{pl},S_{cr},S_{lt})$		→ 0,5;1,5;1,4	451	7/56	+14,2	-	496	52	+13,8
availability factors G_i (1)	G_{pl}		→ 0,88(+10%)	397	12/56	0	-	446	52	+0,8
		0,8	→ 0,72(-10%)	397	12/56	0	-	439	52	-0,8
	G_{cr}		→ 0,55(+10%)	406	9/56	+2,4	-	453	52	+2,3
		0,5	→ 0,45(-10%)	387	9/56	-2,4	-	433	52	-2,3
	G_{lt}		→ 0,33(+10%)	419	9/56	+3,2	-	455	52	+2,8
		0,3	→ 0,27(-10%)	384	9/56	-3,2	-	431	52	-2,8
	$\max(G_{pl},G_{cr},G_{lt})$		→ 0,88;0,55;0,33	423	12/58	+6,5	-	469	52	+5,9
	$\min(G_{pl},G_{cr},G_{lt})$		→ 0,72;0,45;0,27	371	12/58	-6,5	-	417	52	-5,9
zone boundary temperatures T_i (°C)	T_{pl}		→ 1750(+3%)	386	9/58	-2,3	+2	417	52	-4,3
		1700	→ 1650(-3%)	410	7/54	+3,8	-2	455	52	+4,3
	T_{cr}		→ 1350(+4%)	391	7/56	-1	-	431	52	-1
		1300	→ 1250(-4%)	399	7/56	+1	-	440	52	+1
	$\max(T_{pl},T_{cr})$		→ 1750 ,1350	382	7/56	-3,3	+2	412	52	-5,3
	$\min(T_{pl},T_{cr})$		→ 1650, 1250	414	7/54	+4,8	-2	459	52	+5,3
thermal conductivity fuel k (W/cm°C)			→ (+10%)	369	7/60	-6,6	+4	410	52	-6
			→ (-10%)	427	7/52	+8,1	-4	485	52	+11,2
heat trans. coefficient fuel clad h_{hg} (W/cm²°C)			→ 1,5(+36%)	382	9/59	-3,8	+3	415	52	-4,8
		1,1	→ 0,7(-36%)	431	12/52	+8,3	-4	503	52	+13,5
coolant temp. increase ΔT_{Na} (°C)			→ 265(+43%)	402	12/56	+1,2	-	466	52	+5,2
		185	→ 135(-27%)	393	7/56	-1,2	-	420	52	-5,2

Fig. 1 Dependence of the porosity factor $1 - P^{2/3}$ and of the Loeb straight lines on the porosity

Porosity - Relation

$K(T,P) = K_{th}(T)\left[1 - P^{2/3}\right]$

Loeb straight lines

$K(T,P) = K_{th}(T)\left[1 - \eta P\right]$

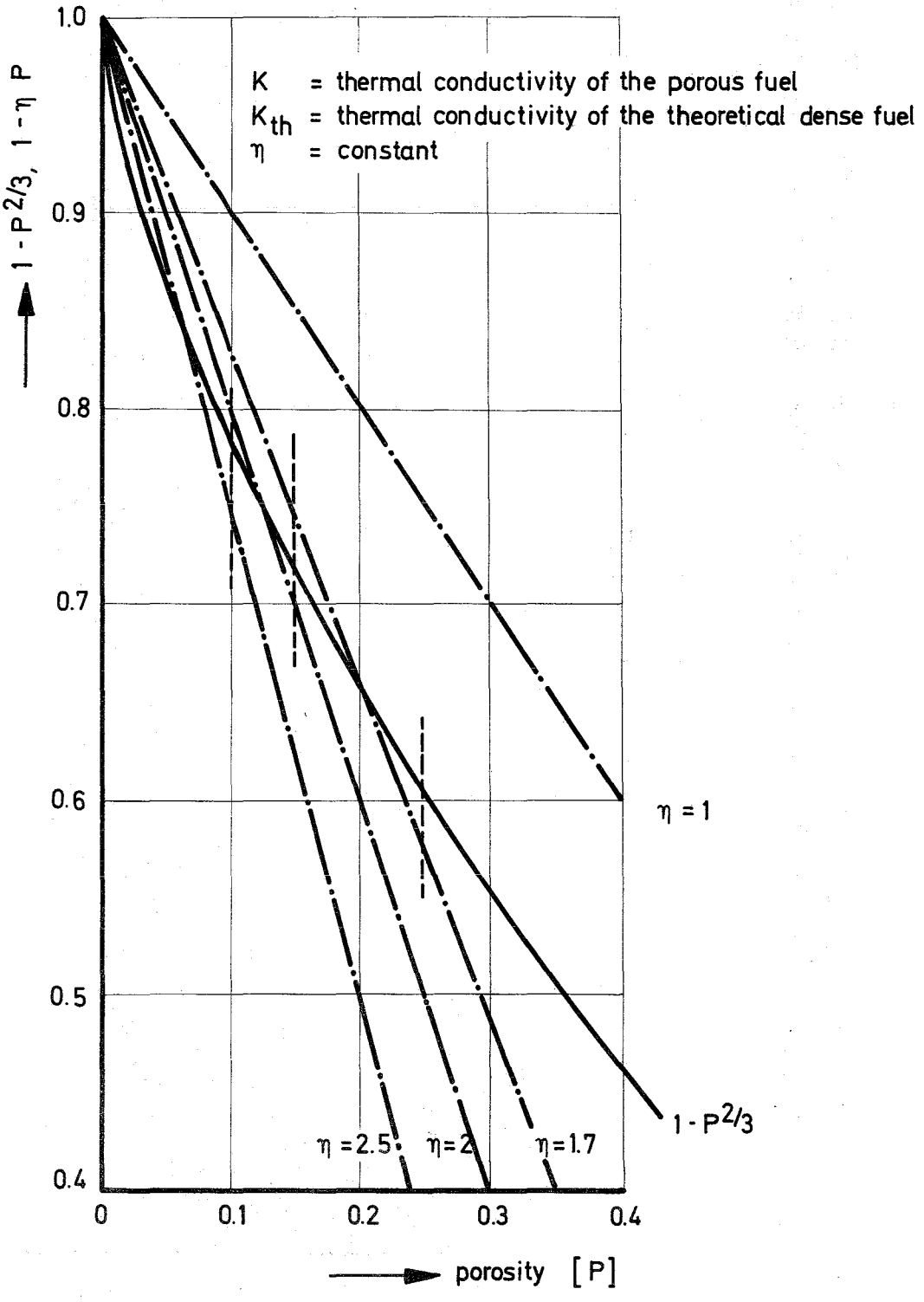

Fig. 2 Thermal conductivity K for stoichiometric UO_2 and $(U_{0,8}\ Pu_{0,2})O_2$ in dependence of the temperature T and porosity P as parameter.

$$K(T,P) = K_{th}(T)\,[1 - P^{2/3}]$$

$$K_{th}(T) = \frac{41.2}{T + 4.9} + 6.55 \cdot 10^{-13}\ T^3 \pm 7\ \% \left[\frac{W}{cm\ °K}\right] \quad T \text{ in } °K$$

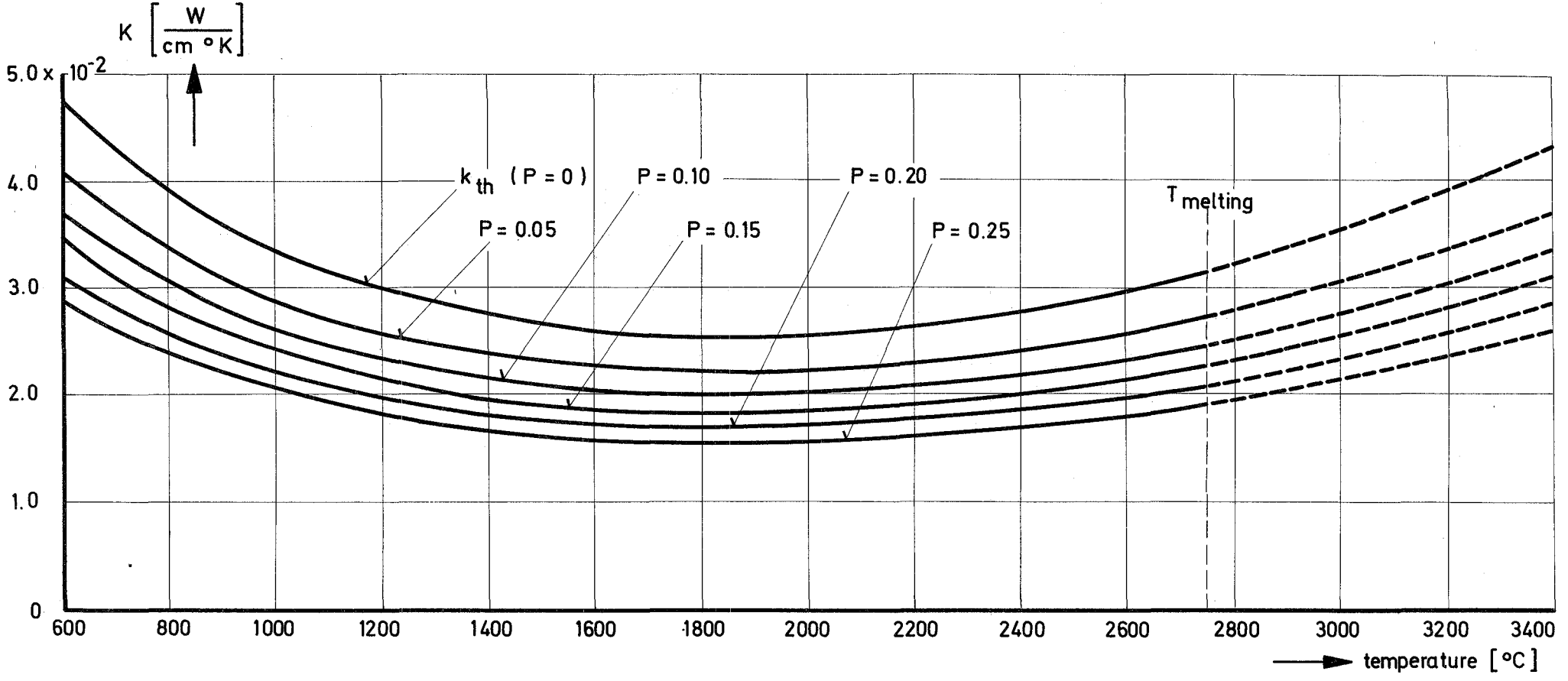

FIG. 4 SWELLING PRESSURE OF THE FUEL IN DEPENDENCE OF THE LINEAR ROD POWER WITH INNER CLADDING TEMPERATURE $T_{sh,in}$ AS PARAMETER.

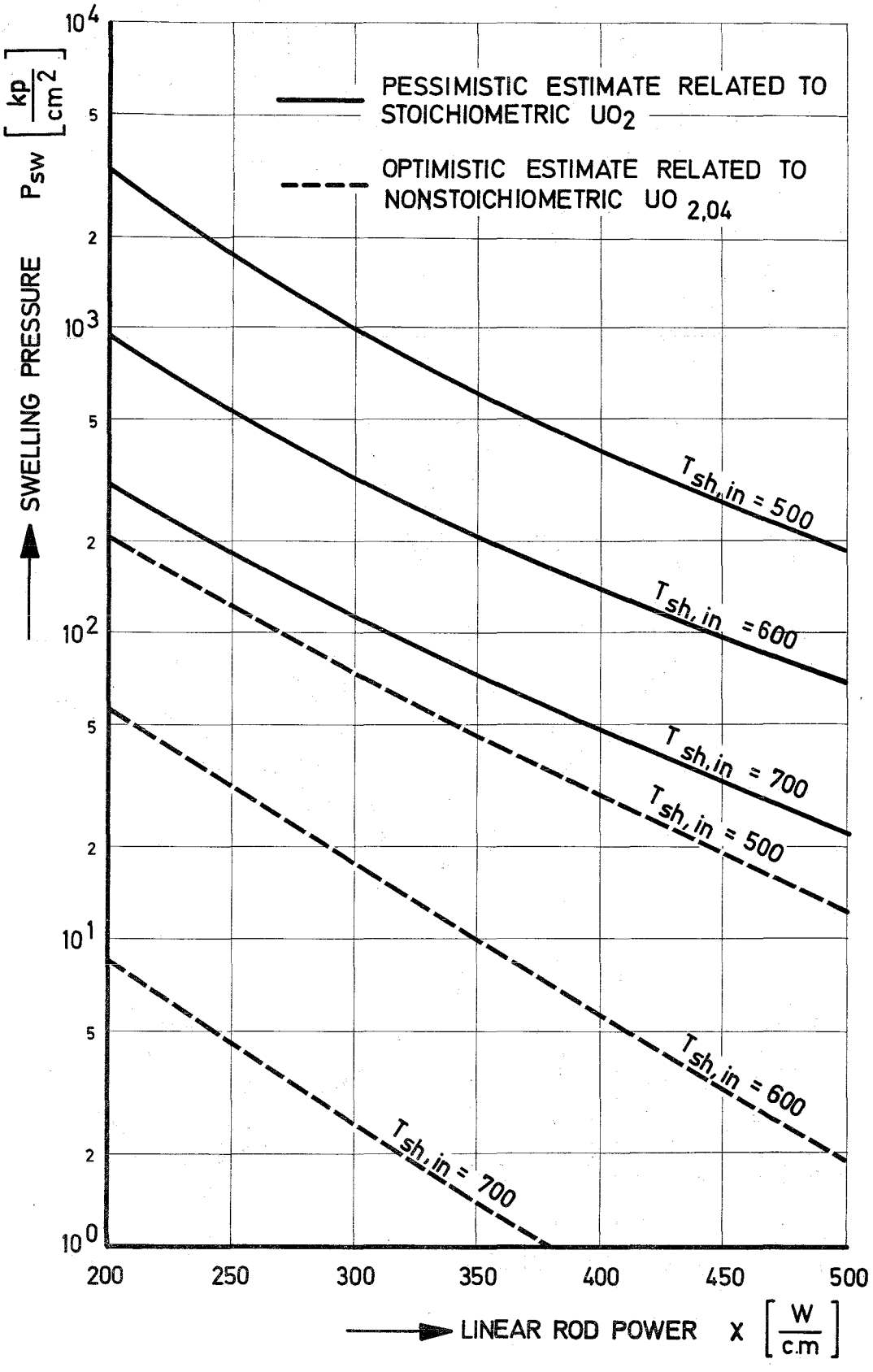

Fig. 5 (Essential) parameter dependences of the maximum operation time t_{max}.

Symbols:

A	=	burnup
d	=	thickness
G	=	availability-factor
h	=	heat transfer coefficient
K	=	thermal conductivity
P	=	porosity
r	=	radius
S	=	swelling rate
T	=	temperature
T.D.	=	temperature distribution
V	=	volume
α	=	thermal expansion coefficient
δ	=	initial gap width
$\varkappa_i$	=	coefficients
χ	=	linear rod power

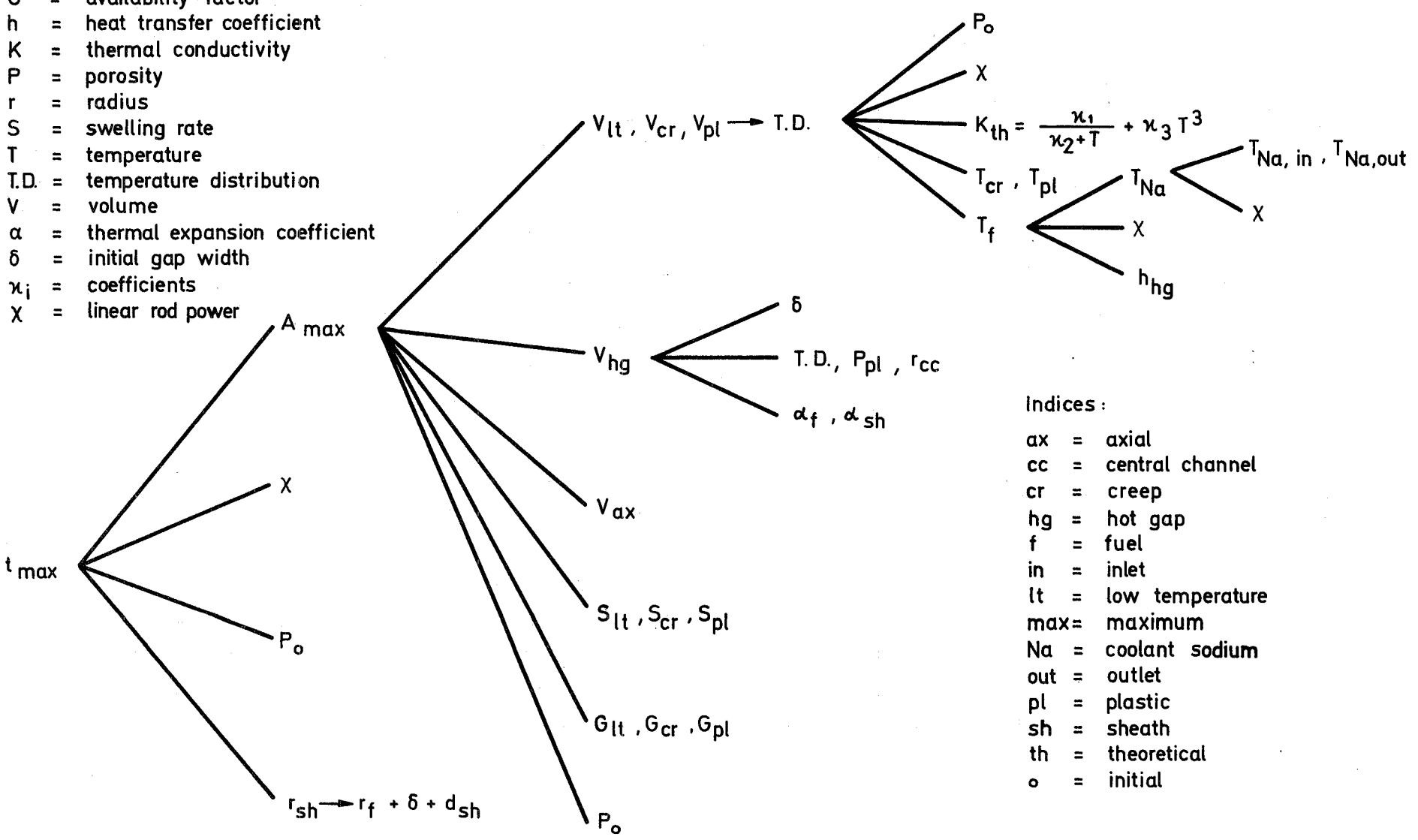

Indices:

ax	=	axial
cc	=	central channel
cr	=	creep
hg	=	hot gap
f	=	fuel
in	=	inlet
lt	=	low temperature
max	=	maximum
Na	=	coolant sodium
out	=	outlet
pl	=	plastic
sh	=	sheath
th	=	theoretical
o	=	initial

Fig. 6 Parameter variation of the burnup-formula for the one-zone-model.

$$A_{max} = \frac{(1 - D_f)\, G + X}{D_f \cdot S} \qquad X = \frac{V_{hg} + V_{ax}}{V_f}$$

Symbols:

A_{max} = maximum burnup
D_f = $1 - P_o$ = relative fuel density
G = availability factor
S = swelling rate
X = relative volume ratio
V_{hg} = hot gap volume
V_{ax} = axial expansion volume
V_f = fuel volume

Normal (averaged) data

G = 0.5
X = 0.05
$S = 1.6 \cdot 10^{-6} \frac{t}{MWd}$

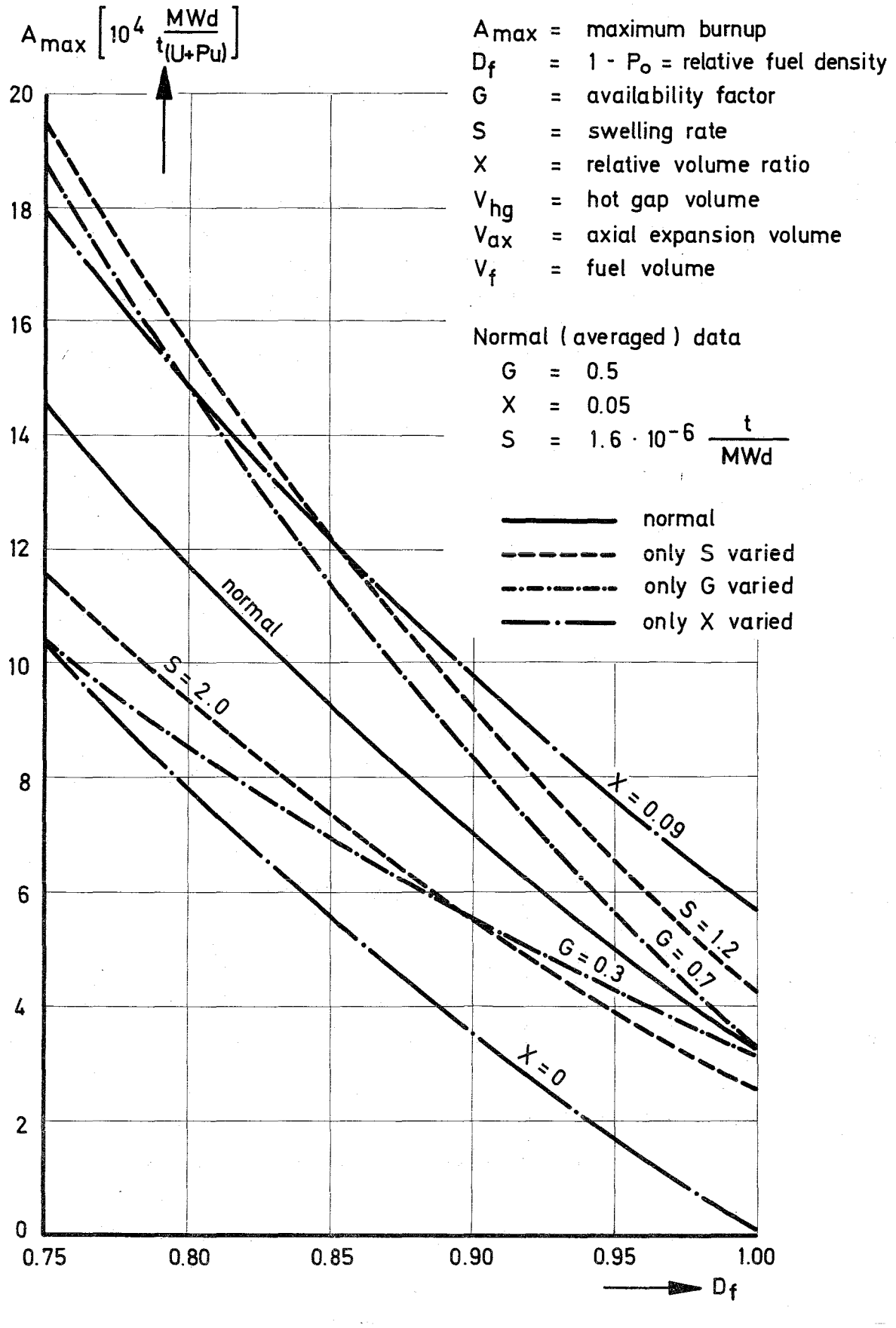

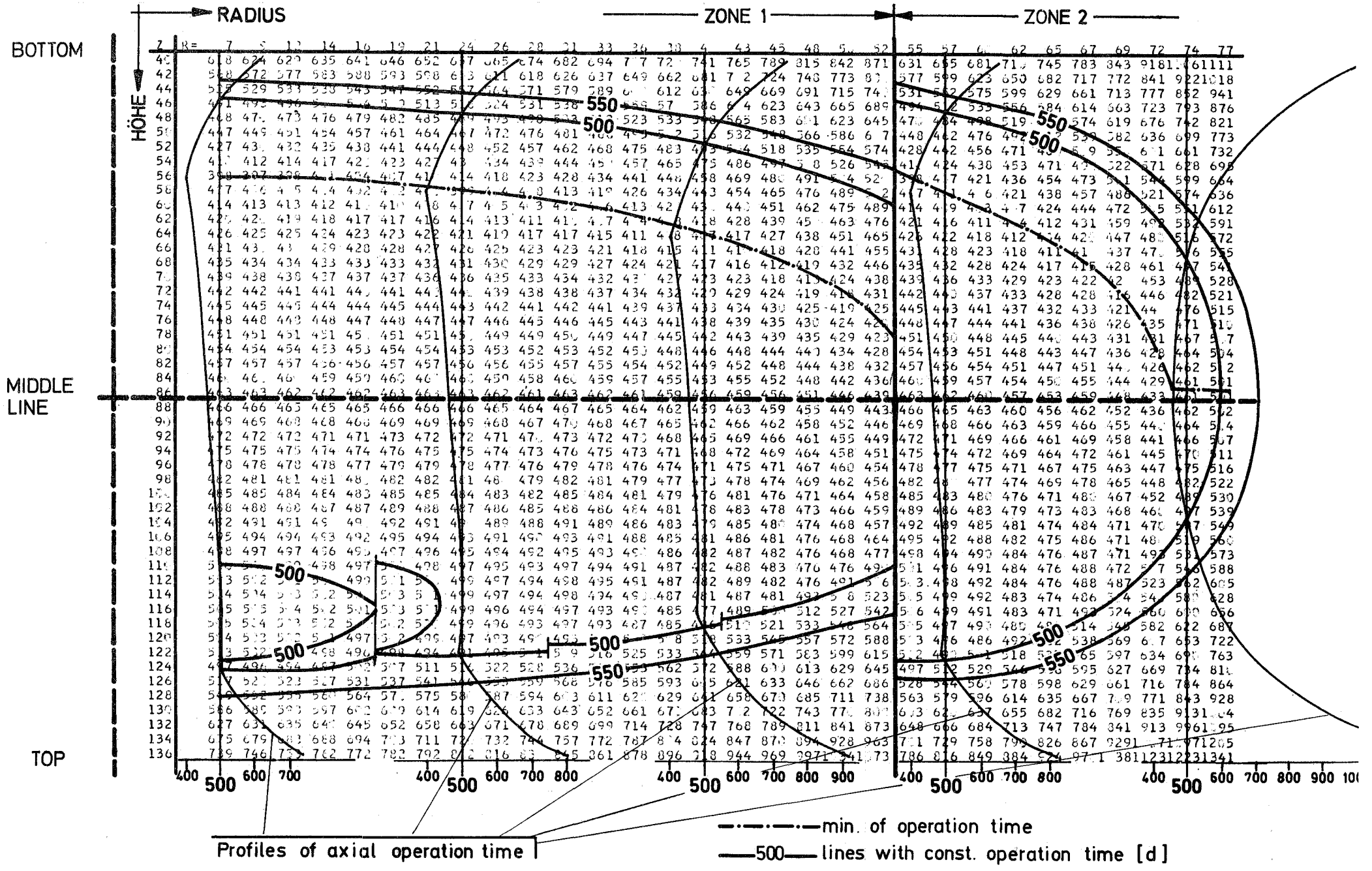

FIG.7 COMPUTER LISTING OF THE MAXIMUM OPERATION TIMES OF THE Na2-CORE

FIG.8 DEPENDENCE OF THE MAXIMUM BURNUP ON THE SMEAR DENSITY WITH LINEAR ROD POWER AND INNER CLAD TEMPERATURE AS PARAMETERS.

CALCULATED ON THE BASE OF THE MATERIAL- AND Na 2 - DATA COMPILED IN TABLE 3

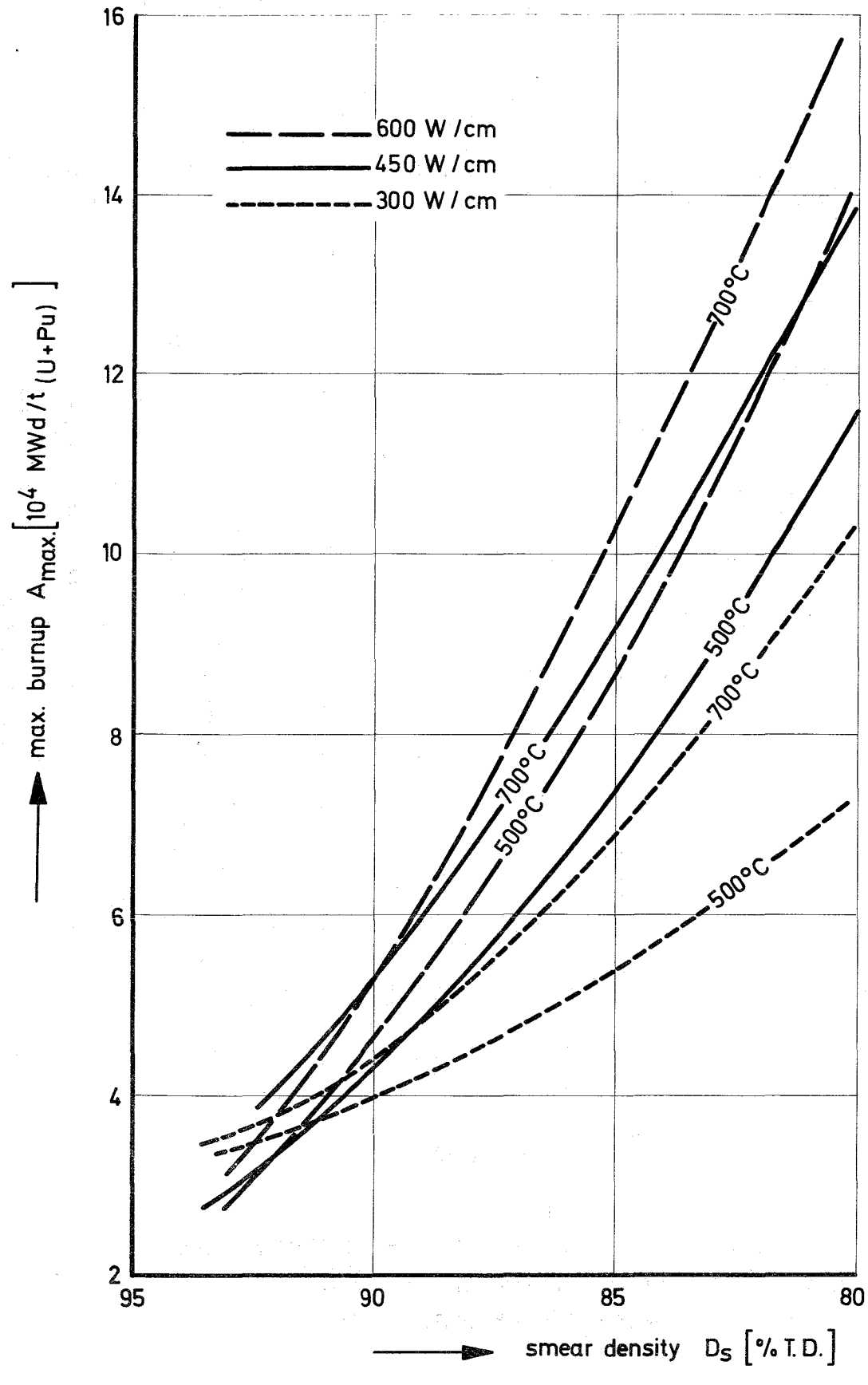

FIG. 9 INTERPRETATION OF THE AXIAL PROFILES OF THE MAXIMUM OPERATION TIMES BY THE RATIOS $\frac{G}{S}$ AND THE AXIAL PROFILES OF THE TEMPERATURE VOLUMES.

ZONE	G_i	$S_i \left[10^{-6}\frac{t}{MWd}\right]$	$\frac{G_i}{S_i}\left[10^{6}\frac{MWd}{t}\right]$
lt	0.3	1.6	0.19
cr	0.5	1.7	0.29
pl	0.8	0.7	1.14

Calculated on the base of the material - and Na 2 - data compiled in table 3 for a position near the core axis.

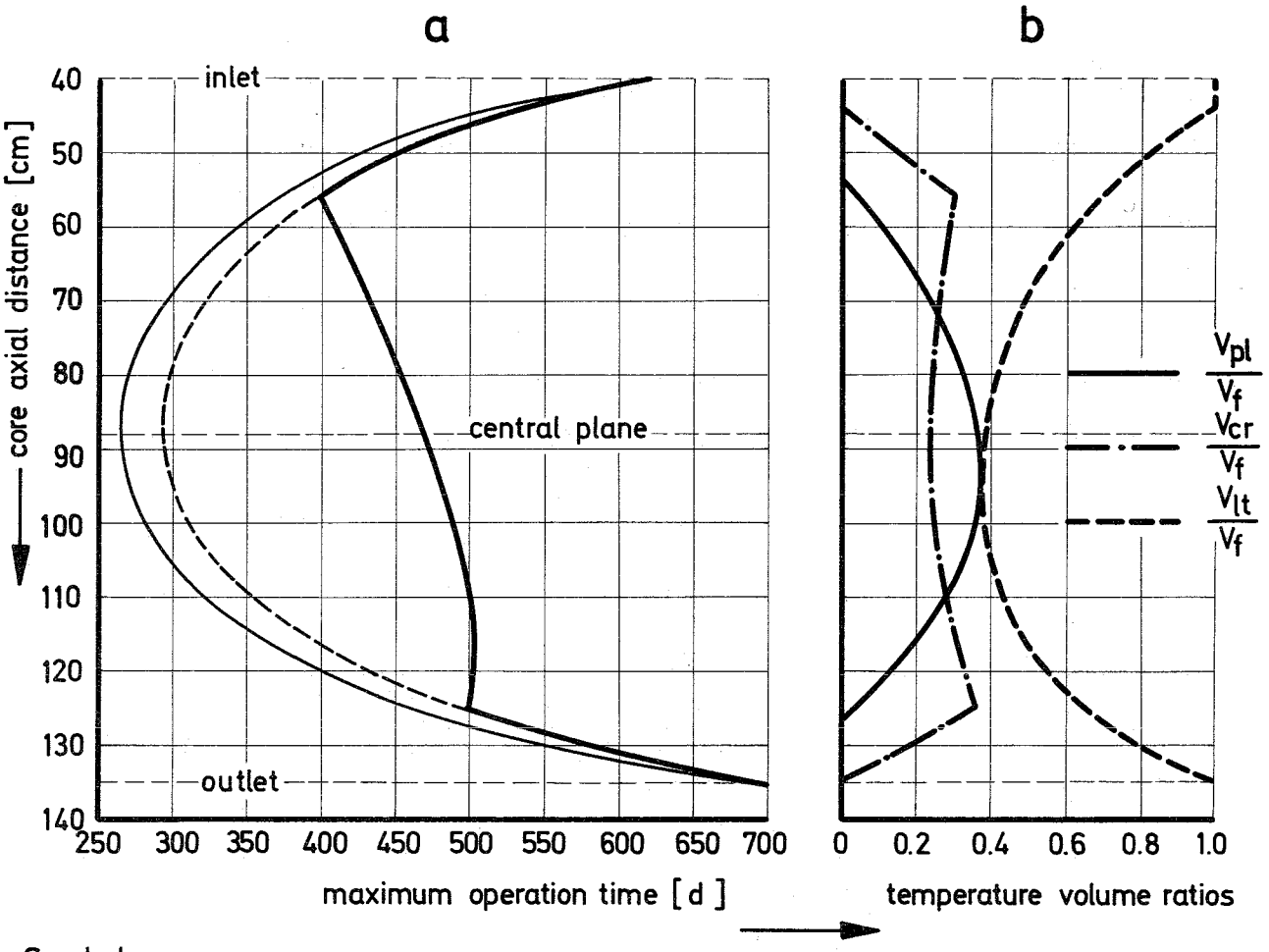

Symbols:

G_i = AVAILABILITY FACTOR
S_i = SWELLING RATE
} i = lt, cr, pl

V_f = FUEL AXIAL VOLUME ELEMENT

V_{lt} = AXIAL VOLUME ELEMENT OF THE LOW TEMPERATURE ZONE

V_{cr} = AXIAL VOLUME ELEMENT OF THE CREEP ZONE

V_{pl} = AXIAL VOLUME ELEMENT OF THE PLASTIC ZONE

FIG. 10 THE INFLUENCE OF THE ZONE SWELLING RATES AND THE AVAILABILITY FACTORS ON THE AXIAL MAXIMUM OPERATION TIME PROFILES.

CASE	LOW TEMPERATURE ZONE			CREEP ZONE			PLASTIC ZONE		
	G	S	$\frac{G}{S}$	G	S	$\frac{G}{S}$	G	S	$\frac{G}{S}$
1=normal	0.3	1.6	0.19	0.5	1.7	0.29	0.8	0.7	1.14
2	0.3	1.6	0.19	0.4	2.0	0.2	0.8	0.7	1.14
3	0.3	1.6	0.19	0.6	1.4	0.43	0.8	0.7	1.14
4	0.3	1.6	0.19	0.5	1.7	0.29	0.6	1.1	0.55
5	0.3	1.6	0.19	0.5	1.7	0.29	0.6	1.5	0.4

CALCULATED ON THE BASE OF THE MATERIAL - AND Na 2 - DATA COMPILED IN TABLE 3 FOR A POSITION NEAR THE CORE AXIS

G = AVAILABILITY FACTOR

S = SWELLING RATE $\left[10^{-6}\ \frac{t}{MWd}\right]$

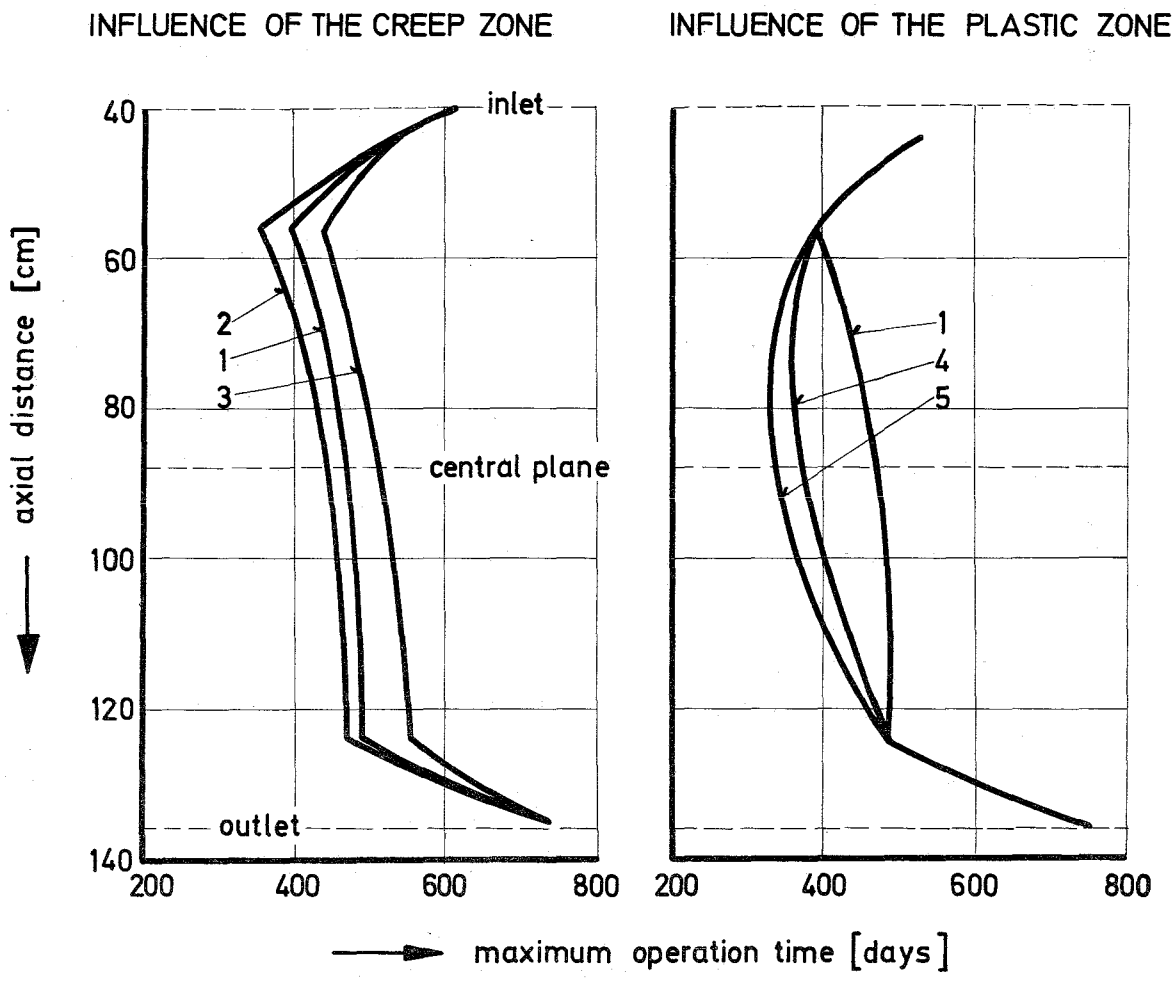

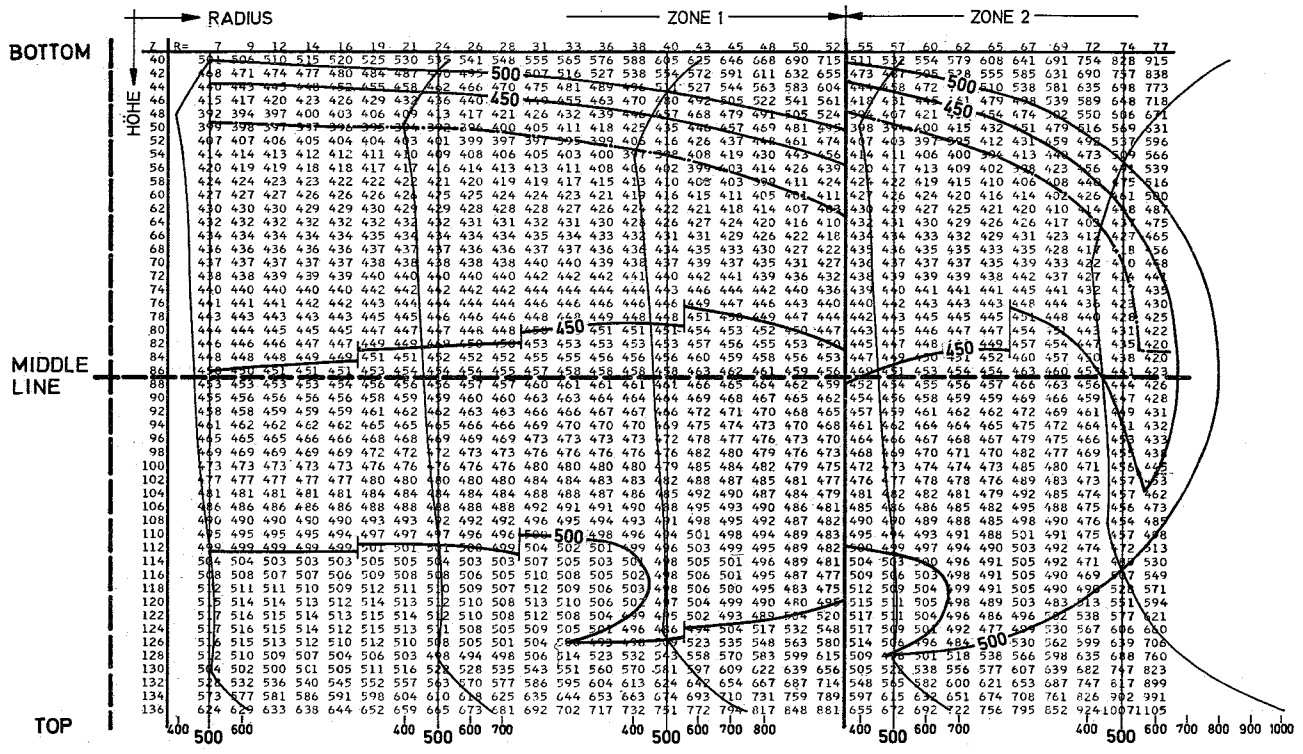

a) $\Delta\chi = +20\%$

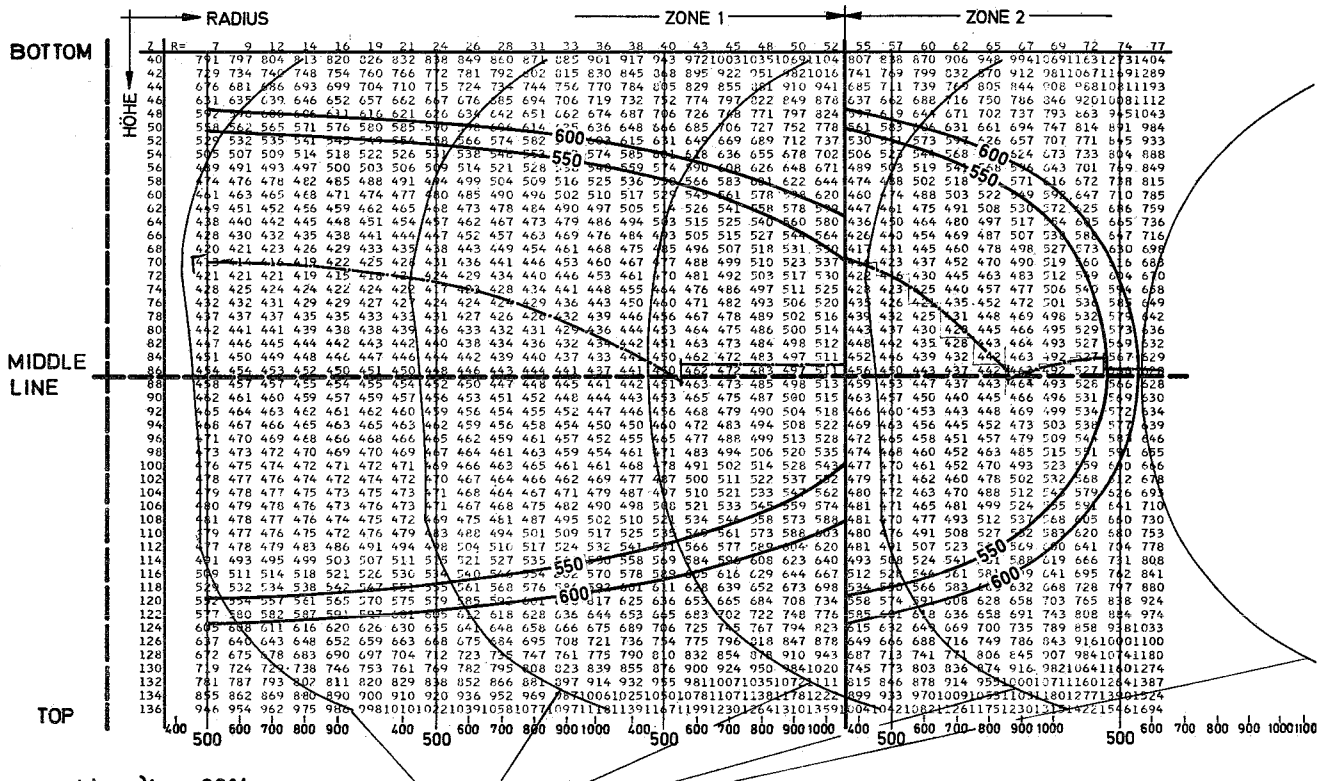

b) $\Delta\chi = -20\%$

Profiles of axial operation time

-·-·-·- min. of operation time

——— lines with const. operation time [d]

RESULT

CASE	ABSOL. MIN. OF OPERATION TIME VALUE [d]	POSITION R/Z [cm]	BELONGING BURNUP IN THE CORE-CENTER [MWd / tM]
a	392	7 / 52	113·000
b	413	7 / 70	79 500

FIG. 11 OPERATION TIME ANALYSIS IN Na 2 - CORE, INFLUENCE OF PARAMETERS CHANGED VALUE OF PARAMETER : ROD POWER

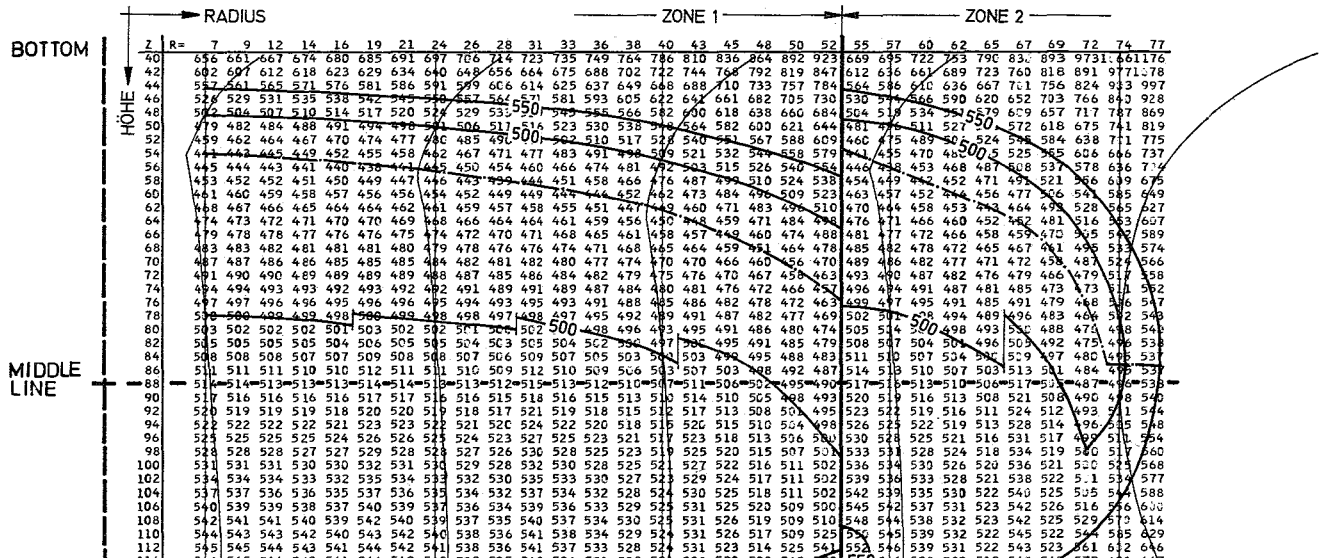

a) Pa = 0,175(+13 %)

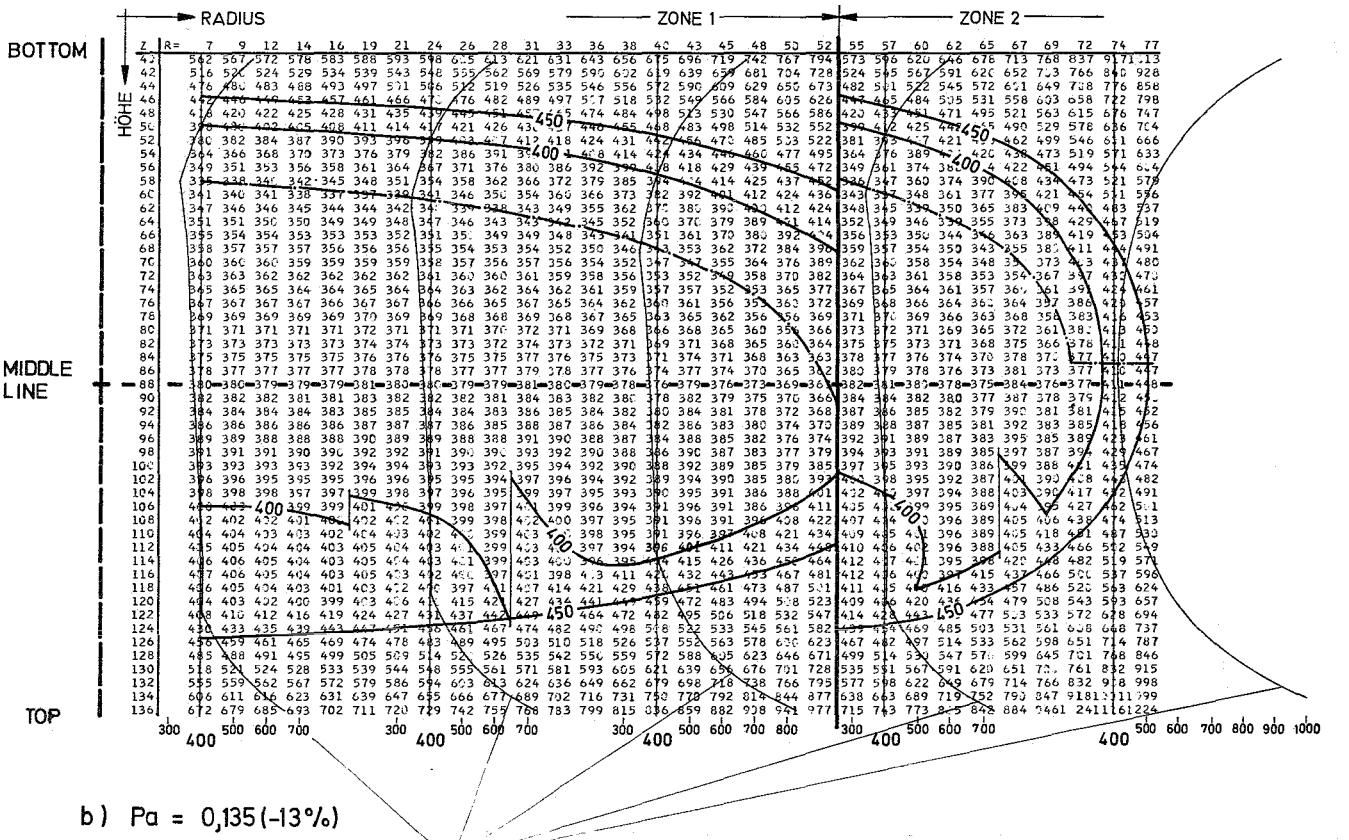

b) Pa = 0,135(-13%)

Profiles of axial operation time

—·—·— min. of operation time

——— lines with const. operation time [d]

RESULT

CASE	ABSOL. MIN. OF OPERATION TIME VALUE [d]	POSITION R/Z [cm]	BELONGING BURNUP IN THE CORE-CENTER [MWd / t M]
a	441	7 / 54	106 600
b	335	7 / 54	81 000

FIG.12 OPERATION TIME ANALYSIS IN Na2-CORE , INFLUENCE OF PARAMETERS CHANGED VALUE OF PARAMETER: FABRICATED FUEL POROSITY

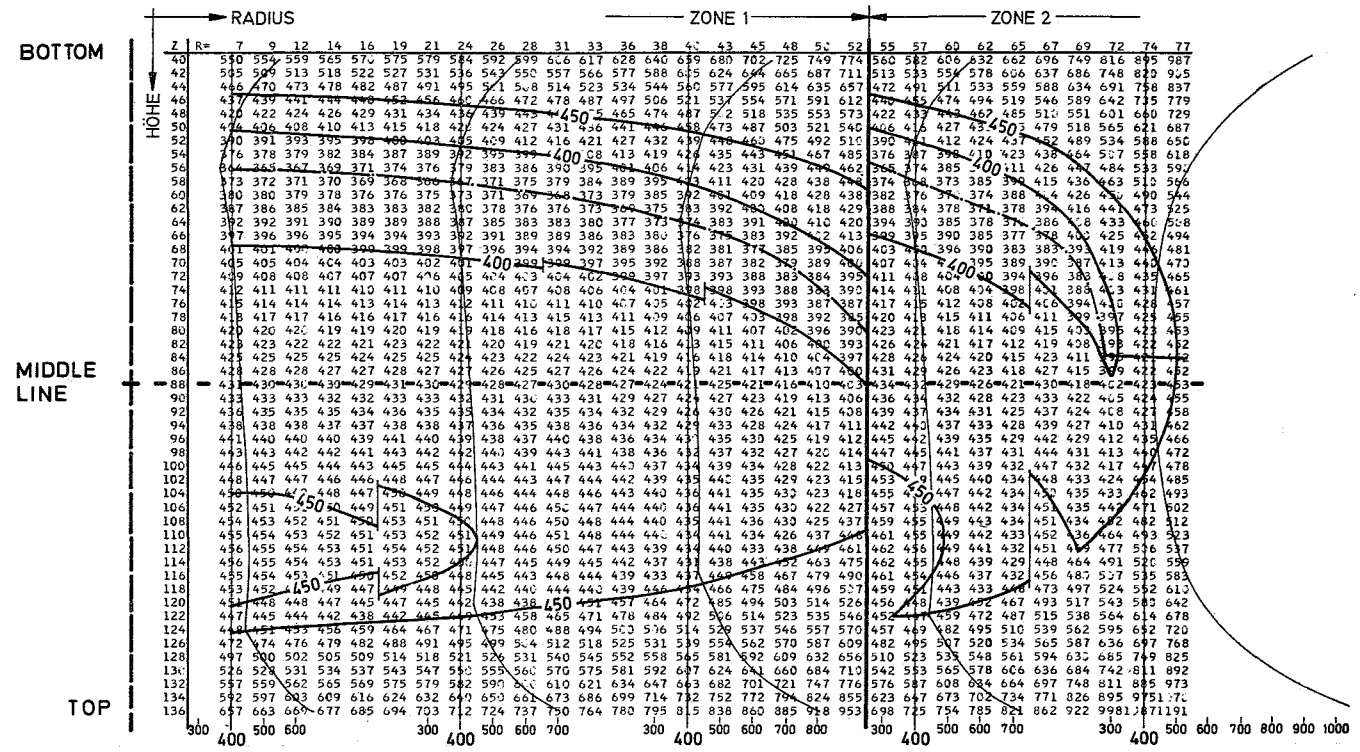

a) $S_{lt} = 1{,}8\left[\frac{v/o}{10^4 MWd/tM}\right] (+13\,\%)$

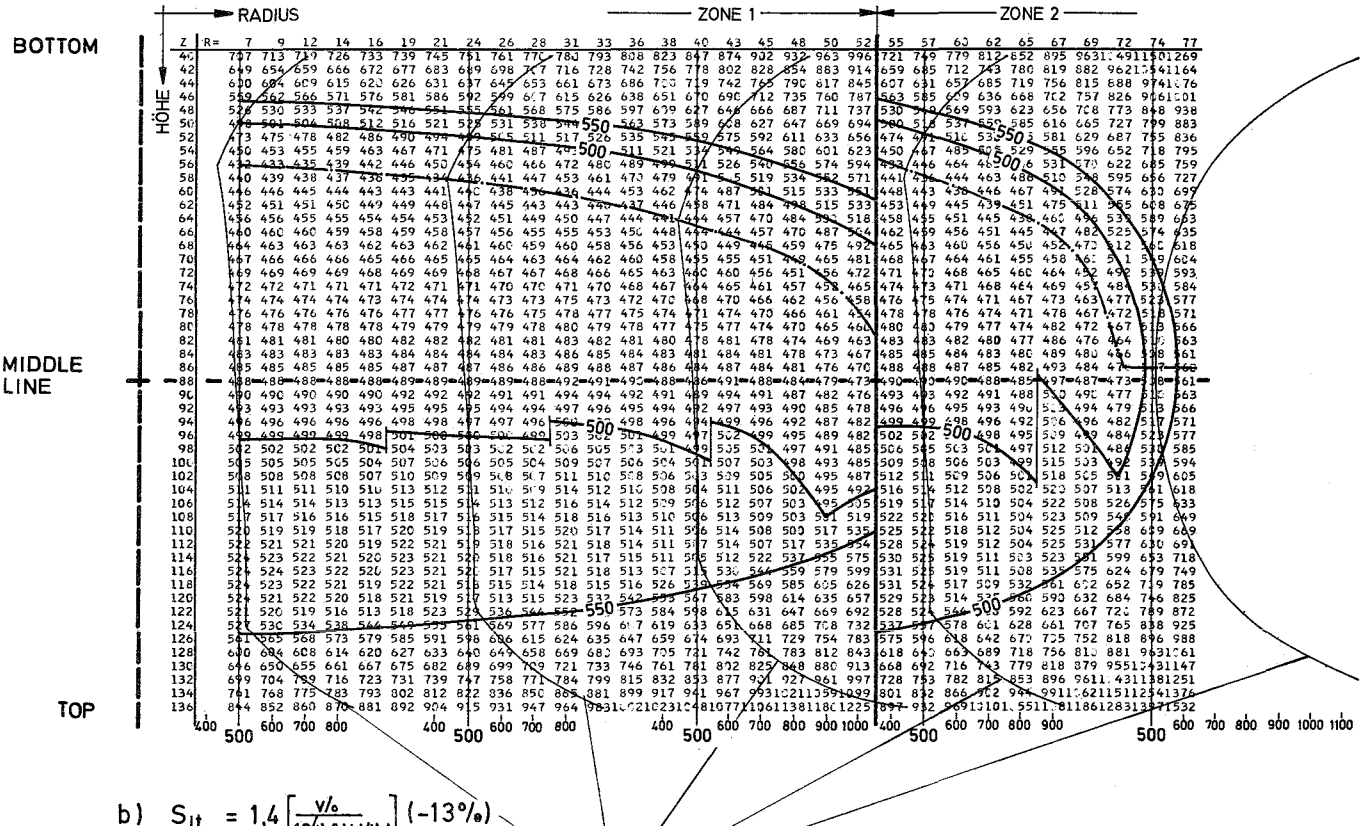

b) $S_{lt} = 1{,}4\left[\frac{v/o}{10^4 MWd/tM}\right] (-13\,\%)$

Profiles of axial operationtime

min. of operationtime

lines with const. operationtime [d]

RESULT :

CASE	ABSOL. MIN OF OPERATIONTIME VALUE [d]	POSITION R/Z [cm]	BELONGING BURNUP IN THE CORE-CENTER [MWd / t M]
a	364	7/ 56	87 400
b	432	7/ 56	10 400

FIG.13 OPERATION TIME ANALYSIS IN Na-2 CORE, INFLUENCE OF PARAMETERS CHANGED VALUE OF PARAMETER: SWELLING RATE LOW TEMP. ZONE

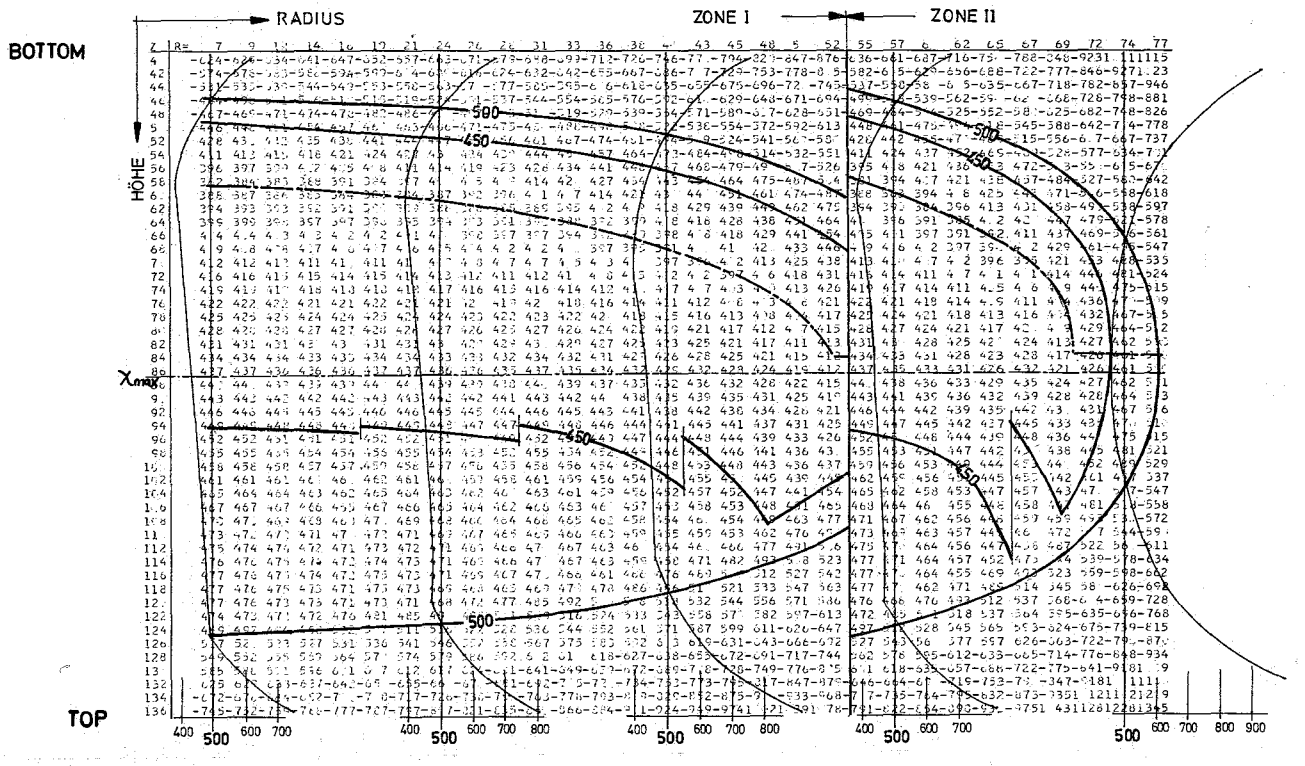

a) $h_{Sp} = 1{,}5\left[\frac{W}{cm^2 \cdot grd}\right](+36\%)$

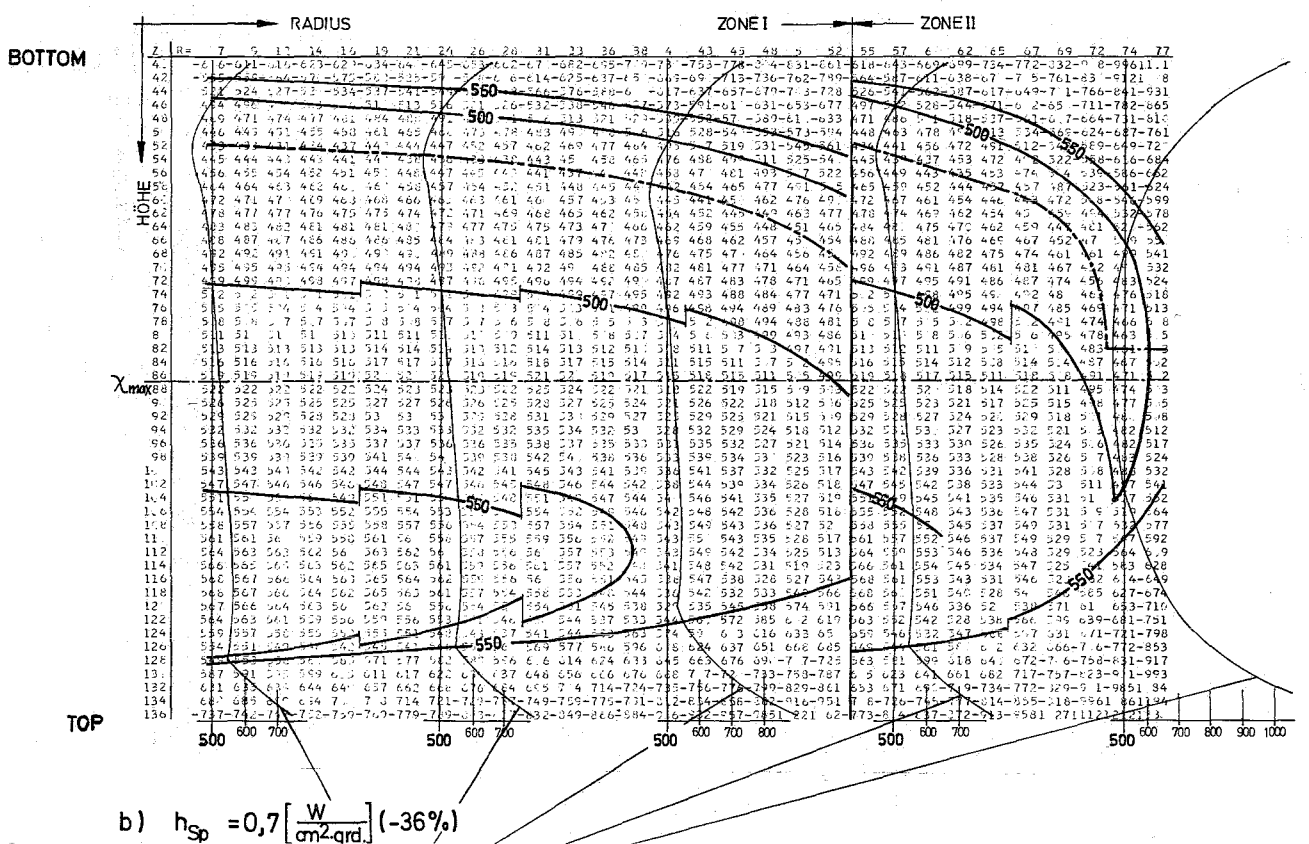

b) $h_{Sp} = 0{,}7\left[\frac{W}{cm^2 \cdot grd.}\right](-36\%)$

RESULT

CASE	ABSOL. MIN. OF OPERATION TIME VALUE [d]	POSITION R/Z [cm]	BELONGING BURNUP IN THE CORE-CENTER [MWd/tM]
a	382	9 / 59	92 000
b	431	12 / 52	103 600

Profiles of axial operation time
——·—— min. of operation time
——— lines with const. operation time [d]

FIG.14 OPERATION TIME ANALYSIS IN Na2-CORE, INFLUENC OF PARAMETERS CHANGED VALUE OF PARAMETER: TRANSFER COEFF. FUEL-CLAD

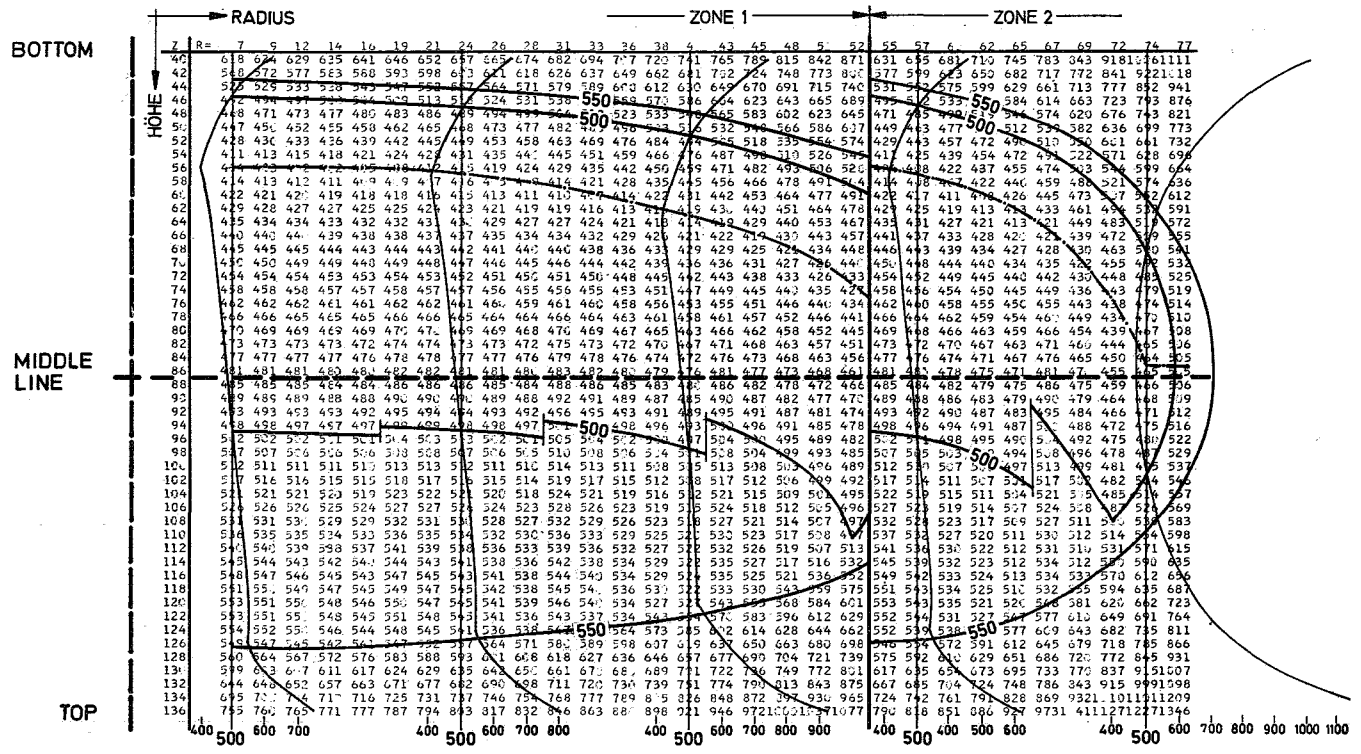

a) $T_{A(Na)} = 650°C\ (+14\%)$

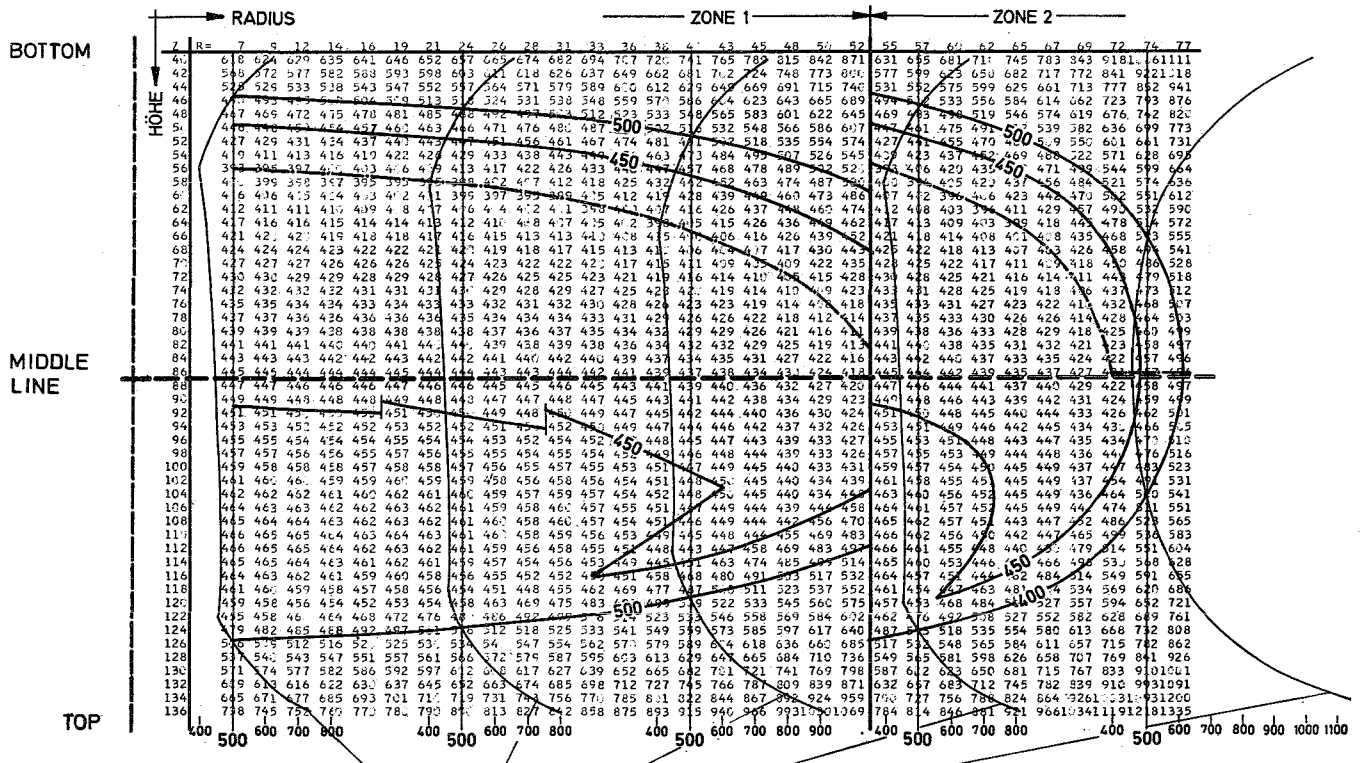

b) $T_{A(Na)} = 520°C\ (-8{,}6\%)$

Profiles of axial operation time

—·—·— min. of operation time

——— lines with const. operation time [d]

RESULT

CASE	ABSOL. MIN. OF OPERATION TIME VALUE [d]	POSITION R/Z [cm]	BELONGING BURNUP IN THE CORE-CENTER [MWd / tM]
a	402	12 / 56	97 200
b	393	7 / 56	94 500

FIG.15 OPERATION TIME ANALYSIS IN Na 2-CORE, INFLUENCE OF PARAMETERS CHANGED VALUE OF PARAMETER: OUTLET TEMPERATURE Na